การตรวจสอบความถูกต้องของหน่วยนับวัดมอนิเตอร์จากการใช้ข้อมูลเครื่องวัดปริมาณรังสีหลาย
ชนิด ในการฉายรังสีโฟตอนขนาดเล็ก สำหรับเครื่องวางแผนการรักษาอีคลิปส์ (ECLIPSE™)

นายแซมมัว มาเมสะ

วิทยานิพนธ์นี้เป็นส่วนหนึ่งของการศึกษาตามหลักสูตรปริญญาวิทยาศาสตรมหาบัณฑิต
สาขาวิชาฉายาเวชศาสตร์ ภาควิชารังสีวิทยา
คณะแพทยศาสตร์ จุฬาลงกรณ์มหาวิทยาลัย
ปีการศึกษา 2560
ลิขสิทธิ์ของจุฬาลงกรณ์มหาวิทยาลัย

MONITOR UNIT (MU) VALIDATION USING VARIOUS TYPES OF DOSIMETERS FOR

COMMISSIONING SMALL FIELD IN ECLIPSE™ TREATMENT PLANNING SYSTEM

Mr. Sammuel Mamesa

จุฬาลงกรณ์มหาวิทยาลัย
CHULALONGKORN UNIVERSITY
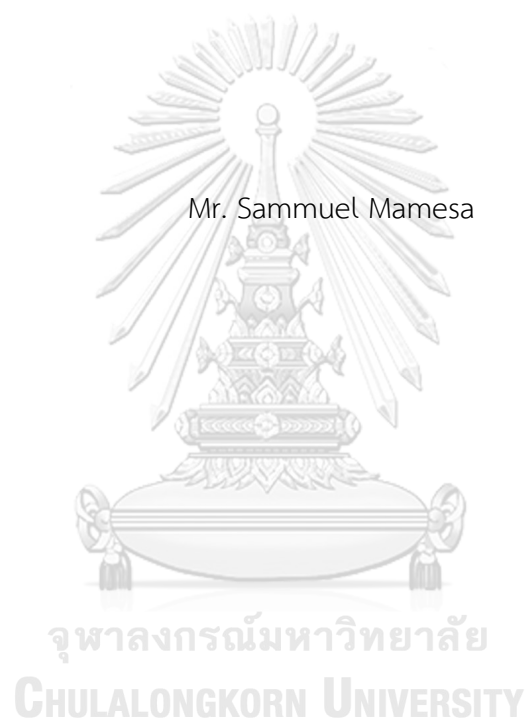
A Thesis Submitted in Partial Fulfillment of the Requirements

for the Degree of Master of Science Program in Medical Imaging

Department of Radiology

Faculty of Medicine

Chulalongkorn University

Academic Year 2017

Thesis Title	MONITOR UNIT (MU) VALIDATION USING VARIOUS TYPES OF DOSIMETERS FOR COMMISSIONING SMALL FIELD IN ECLIPSE™ TREATMENT PLANNING SYSTEM
By	Mr. Sammuel Mamesa
Field of Study	Medical Imaging
Thesis Advisor	Associate Professor Sivalee Suriyapee, M.Eng

Accepted by the Faculty of Medicine, Chulalongkorn University in Partial Fulfillment of the Requirements for the Master's Degree

....Dean of the Faculty of Medicine

(Professor Suttipong Wacharasindhu, M.D.)

THESIS COMMITTEE

....Chairman

(Mr. Taweap Sanghangthum, Ph.D.)

....Thesis Advisor

(Associate Professor Sivalee Suriyapee, M.Eng)

....Examiner

(Mr. Isra Israngkul Na Ayuthaya, Ph.D.)

....External Examiner

(Professor Franco Milano, Ph.D.)

แซมมัว มาเมสะ : การตรวจสอบความถูกต้องของหน่วยนับวัดมอนิเตอร์จากการใช้ข้อมูล
เครื่องวัดปริมาณรังสีหลายชนิด ในการฉายรังสีโฟตอนขนาดเล็ก สำหรับเครื่องวางแผนการรักษา
อีคลิปส์ (ECLIPSE™) (MONITOR UNIT (MU) VALIDATION USING VARIOUS TYPES OF
DOSIMETERS FOR COMMISSIONING SMALL FIELD IN ECLIPSE™ TREATMENT
PLANNING SYSTEM) อ.ที่ปรึกษาวิทยานิพนธ์หลัก: ศิวลี สุริยาปี, 72 หน้า.

วัตถุประสงค์ของการศึกษานี้ เพื่อตรวจสอบความแตกต่างของจำนวน monitor unit ที่คำนวณ
จากข้อมูลที่ใส่ในเครื่องวางแผนการรักษา โดยใช้ค่า field output factors ที่ได้แก้ค่าแล้วของหัววัดรังสีแต่
ละชนิด เปรียบเทียบกับค่าที่ได้จากการเฉลี่ยของค่า field output factors จากเครื่องวัดรังสีสามชนิดที่
ไม่ได้แก้ค่าหัววัดรังสี การเก็บข้อมูลของ percentage depth doses และ beam profiles ได้แก่ IBA
CC01, IBA PFD, IBA EFD และ Sun Nuclear Edge โดยใช้ลำรังสีโฟตอน 6 ล้านโวลต์ แบบลำรังสีเรียบ
ขนาดจาก 1x1 ซม^2 ถึง 10x10 ซม^2 การวัด field output factors ใช้เพียง 3 หัววัด โดยตัด Edge
detector ออก การคำนวณ field output factors ใช้สองวิธีคือการแก้ค่าตาม IAEA/AAPM TRS398 และ
ไม่แก้ค่า เมื่อเก็บข้อมูลการวัดรังสีแล้ว จึงใส่ไปในเครื่องวางแผนการรักษา Eclipse ซึ่งการคำนวณใช้
Acuros XB algorithm โดยจัดทำข้อมูล 4 ชุด การตรวจสอบทำใน 6 พื้นที่ลำรังสีแบบสมมาตร การฉาย
รังสีแบบผ่าตัดเทคนิคปรับความเข้ม 10 แผนการรักษา แบบผ่าตัดเทคนิคปรับความเข้มหมุนรอบตัว 10
แผนการรักษา ผลการวัด depth dose curves และ beam profiles ในทุกหัววัดมีค่าใกล้เคียงกัน ส่วน
beam profile จะกว้างเมื่อวัดจาก CC01 ค่า field output factors ของ PFD สูงกว่าค่าเฉลี่ยจากหัววัด
สามตัวที่ไม่ได้แก้ค่าในทุกขนาดลำรังสี ส่วน EFD และ CC01 ได้ค่าใกล้เคียง จนกระทั่งถึงขนาดลำรังสี
1.5x1.5 ซม^2 และ 1x1 ซม^2 ตามลำดับ ค่าในการคำนวณ MU ด้วยโปรแกรมจากเครื่องวางแผน Eclipse
ในลำรังสีสมมาตรพบว่า ความแตกต่างจากการคำนวณด้วยค่าเฉลี่ยจากเครื่องวัดรังสีสามชนิดที่ไม่ได้แก้ค่า
เท่ากับ 0.2%, -1.6% และ 1.2% ในการวัดด้วย CC01, PFD และ EFD ที่แก้ค่าแล้ว ตามลำดับ ส่วนการวาง
แผนการรักษาเทคนิคปรับความเข้ม ความแตกต่างเท่ากับ -1.3%, -3.4% และ -1.5% และแบบปรับความ
เข้มหมุนรอบตัว ความแตกต่างเท่ากับ 0.2%, 2.0% และ -0.2% ตามลำดับ

ภาควิชา รังสีวิทยา	ลายมือชื่อนิสิต ....
สาขาวิชา ฉายาเวชศาสตร์	ลายมือชื่อ อ.ที่ปรึกษาหลัก ....
ปีการศึกษา 2560	

5974112030 : MAJOR MEDICAL IMAGING

KEYWORDS: FIELD OUTPUT FACTORS / MONITOR UNIT / SMALL FIELD DOSIMETRY / IAEA/AAPM TRS 483

SAMMUEL MAMESA: MONITOR UNIT (MU) VALIDATION USING VARIOUS TYPES OF DOSIMETERS FOR COMMISSIONING SMALL FIELD IN ECLIPSE™ TREATMENT PLANNING SYSTEM. ADVISOR: ASSOC. PROF. SIVALEE SURIYAPEE, M.Eng, 72 pp.

The objective of this study was to investigate the differences of calculated MU between commissioning using corrected FOF from single detector and commissioning using average uncorrected FOF from three detectors. Measurements were carried out on 6 MV flattened photon beams from 1x1 cm^2 to 10x10 cm^2. Four detectors were utilized to measure depth doses and beam profiles: IBA CC01, IBA PFD, IBA EFD and Sun Nuclear EDGE. For FOF determination, Sun Nuclear EDGE was not used. The determination of FOF was classified into corrected FOF according to IAEA/AAPM TRS 483 and uncorrected FOF from three detectors. Commissioning was undertaken in Eclipse™, and Acuros XB was selected as the dose calculation algorithm. Four beam commissioning datasets were generated. The validation of calculated MU was made in 6 symmetric field sizes, 10 IMRT-SRS plans and 10 VMAT-SRS plans. It was observed that in depth dose curves and beam profiles, the outcomes among all detectors were relatively similar although broader penumbra from CC01 was noted. For FOF, corrected PFD showed higher outcome than the average uncorrected FOF in all field sizes while the corrected EFD and corrected CC01 were agreeable to 1.5x1.5 cm^2 and 1x1 cm^2, respectively. In symmetric fields, validation of MU yielded mean differences of 0.2%, -1.6% and 1.2% for commissioning using corrected CC01, corrected PFD and corrected EFD, respectively. For validation in IMRT-SRS plans, the mean differences were -1.3%, -3.4% and -1.5%, respectively. For validation in VMAT-SRS plans, the mean differences were 0.2%, 2.0% and -0.2%, respectively.

Department: Radiology	Student's Signature ....
Field of Study: Medical Imaging	Advisor's Signature ....
Academic Year: 2017	

ACKNOWLEDGEMENTS

CONTENTS

จุฬาลงกรณ์มหาวิทยาลัย

CHULALONGKORN UNIVERSITY

List of Figures

List of Tables

List of Abbreviations

Abbreviations	Terms
AAA	Analytical anisotropic algorithm
AXB	Acuros XB algorithm
CoP	Code of practice
d_{max}	Depth of maximum dose
DVH	Dose volume histogram
FOF	Field output factors
FFF	Flattening filter free
FWHM	Full width at half maximum
IAEA	International atomic energy agency
IGRS	Image guided radiosurgery
IGRT	Image guided radiotherapy
IMRT	Intensity modulated arc therapy
LBTE	Linear boltzman transfer equation
LCPE	Lateral charged particle equilibrium
Linac	Linear accelerator
MLC	Multi leaf collimator
MU	Monitor unit
OAR	Off-axis-ratio
PDD	Percentage depth dose
QA	Quality assurance
r_{lcpe}	Range of lateral charged particle equilibrium
r_{cyl}	Internal radius of cylindrical ion chamber
S_{clin}	Equivalent square field size
SBRT	Stereotactic body radiation therapy
SRS	Stereotactic radiosurgery
SSD	Source to surface distance
SRT	Stereotactic radiotherapy

TG	Task group
TPR	Tissue-phantom ratio
TPS	Treatment planning system
TRS	Technical reports series
TSF	Tissue-scatter factor
VMAT	Volumetric modulated arc therapy
WFF	With flattening filter

CHAPTER I

INTRODUCTION

1.1 Background and rationale

The concept of small field has been widely implemented in radiation therapy over the past decades. The large amount of radiation dose could be delivered precisely to the small lesion which is considered unreachable for the conventional radiation therapy. The stereotactic radiosurgery (SRS), stereotactic radiotherapy (SRT), and stereotactic body radiation therapy (SBRT) are the examples of radiation therapy treatments which are completed in a single fraction or few fractions within large dose of the order 10-25 Gy under the condition of small irradiation field in order to precisely focus the beam to small target. [1] Not only implemented in Linear Accelerator, but also few sophisticated equipments utilize the concept of small field such as Cyber Knife®, Gamma Knife™, and TomoTherapy®. [2]

Despite of its advantageous, the dosimetry issue on small field remains as a challenge. [3] There are three major problems to characterize the small field. [4] The first is lack of lateral charged particle equilibrium (LCPE). This problem occurs when the size of the field turns smaller than the range of lateral charged particle equilibrium (r_{lcpe}). The second problem is partial source occlusion from the collimating devices which corresponds to an overlapping penumbra. The third obstacle is associated to the selection of an appropriate detector. Problems due to the volume averaging effect and perturbation effect are more pronounced as the field size decreases. Previous work reported discrepancy within ±14% among various types of detectors to determine the small field output factors. [5] The detector choice for measuring small field output becomes clearly cumbersome. [6]

Several detectors such as ionization chambers and diode detectors have been developed specifically in accordance to the demand of small field dosimetry. The ionization chambers which are typically used in external beam radiotherapy provide an energy independence and dose rate independence. However, ion chamber is found to underestimate the output due to the volume averaging effect as a

consequence of large size of collecting volume. [7] The volume averaging effect is an effect attributed to the corresponding signal from detector relative to the mean absorbed dose over its sensitive volume. When the beam radius is smaller than the detector size, the signal will be averaged incorrectly and eventually lead to the underestimation of measured dose. [8] The other detector, diode, has been reported as the promising detector for small field. [9] Diode detectors possess small active volume, excellent spatial resolution, and high sensitivity. However, high energy dependence and angular dependence become the drawbacks of employing diode. Presence of encasuplating material with high atomic number and density also introduces another problem related to the perturbation effect in small field. [10] [11]

Furthermore, reference conditions from the existing Code of Practice (CoP) such as AAPM TG 51 and IAEA TRS 398 are unable to be realized in those equipments mentioned above. Recently, an International working group consists of the IAEA and AAPM has released Technical Reports Series (TRS) Number 483 as the latest guideline for small field dosimetry.[4] One of the main points from this Code of Practice (CoP) is the recommendation to apply field output correction factors ($k_{Q_{clin}Q_{msr}}^{f_{clin}f_{msr}}$) to accurately determine the output factors in small field ($\Omega_{Q_{clin}Q_{msr}}^{f_{clin}f_{msr}}$).

Prior to the establishment of this protocol, Alfonso et al has introduced a new systematic approach to determine the absorbed dose in water for small and non-standard clinical fields ($D_{w,Q_{clin}}^{f_{clin}}$) in equation 1.1 [12]:

$$D_{w,Q_{clin}}^{f_{clin}} = D_{w,Q_{msr}}^{f_{msr}} \Omega_{Q_{clin},Q_{msr}}^{f_{clin},f_{msr}} \qquad (1.1)$$

where the $D_{w,Q_{msr}}^{f_{msr}}$ refers to the absorbed dose in water for machine specific reference field size (f_{msr}) with a given beam quality (Q_{msr}). The terms field output factors ($\Omega_{Q_{clin}Q_{msr}}^{f_{clin}f_{msr}}$) was introduced as the ratio of the detector reading at clinical field size ($M_{Q_{clin}}^{f_{clin}}$) relative to the detector reading at machine specific reference field size ($M_{Q_{msr}}^{f_{msr}}$). The field output correction factors ($k_{Q_{clin}Q_{msr}}^{f_{clin}f_{msr}}$) was proposed as a quantity to correct the ratio according to the equation 1.2 as follows:

$$\Omega_{Q_{clin},Q_{msr}}^{f_{clin},f_{msr}} = \frac{M_{Q_{clin}}^{f_{clin}}}{M_{Q_{msr}}^{f_{msr}}} k_{Q_{clin},Q_{msr}}^{f_{clin},f_{msr}} \tag{1.2}$$

In the treatment planning system (TPS), the field output factors (FOF) will be used as the entry data for beam commissioning. Incorrectly measured output factors for commissioning small field can result in the erroneous calculation of monitor unit (MU) which could jeopardize patients during the treatment. [13] Despite of this important statement, concern to address this issue in small field has not been made so far.

The aim of this research was to observe the differences of calculated MU in treatment planning system between commissioning using uncorrected field output factors and corrected field output factors based on IAEA/AAPM TRS 483.

1.2 The scope of thesis

This research covers the determination of output factors in small field by using several types of detectors for TPS commissioning to compute Monitor Unit in Eclipse™ TPS.

1.3 Keywords

Beam commissioning, Field output factors, Monitor Unit, Small field dosimetry, IAEA/AAPM TRS 483.

CHAPTER II

LITERATURE REVIEW

2.1 Theories

2.1.1 Small field radiation therapy

Field size in small field is pair of dimensions (rectangular fields) or diameter (circular fields) which defines the area of field at the certain distance of measurement. It is strongly advised that the distance should be made at full width at half maximum (FWHM) of lateral beam profile measured at 10 cm depth. This depth is generally accepted as the depth where the contribution of contaminating electrons is considerably small. [4] Small field is created by the downstream collimation of either flattened or unflattened photon beams. There are three major problems to characterize the small field as mentioned below. [4] [14]

a. Loss of lateral charged particle equilibrium (LCPE) on the central beam axis.

b. Partial occlusion of the photon source by the collimating devices.

c. Detector related conditions.

The first two problems are related to the beam conditions while the last problem is associated to the selection of detector. At least one of the conditions is fulfilled for an external photon beam to classify the terms of small field. [4]

- **Loss of LCPE on the central beam axis**

One of the main concerns in small feld is loss of LCPE. The existence of LCPE is needed to calculate the dose from collission kerma in the treatment volume of a given medium. [15] The charged particle equilibrium is the condition where the secondary electrons in the specified volume deposit energy outside the ion-collection region are balanced with the secondary electrons produced outside specified volume and deposit their energy inside ion-collection region. Shortly, the ionization loss is compensated by the number of ionization gained. [16] When the beam half width or beam radius is smaller than the range of lateral charged particle equilibrium, the loss of LCPE starts to exist. The range of lateral charged particle

equilibrium depends on several factors such as beam energy, composition as well as the density of medium where the beam penetrates. [3] Figure 2.1 illustrates the range of lateral charged particle equilibrium in water as a function of beam energy which was described by Li et al. [17] Moreover, their work introduced an empirical formula to calculate r_{lcpe} as a function of tissue phantom ratio (TPR_{10}^{20}). Table 2.1 exhibits the range of secondary electrons from each beam energy following equation 2.1.

$$r_{lcpe}\left(\frac{g}{cm^2}\right) = 5.973(TPR_{10}^{20}) - 2.688 \qquad\qquad (2.1)$$
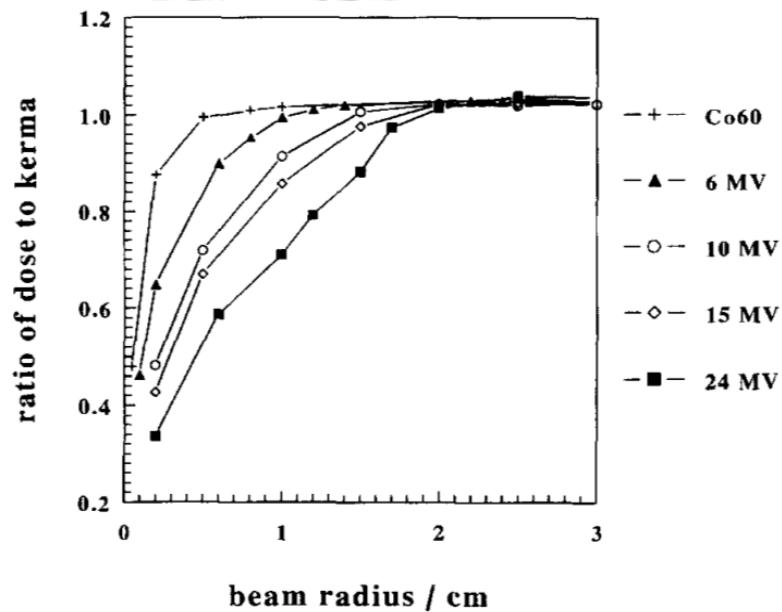
Figure 2.1 Range of secondary electrons for various beam energies to achieve the electronic equilibrium.

Table 2. 1 Value of range of secondary electrons for various beam energies.

Beams	TPR^{20}_{10}	r_{lcpe} ($^g/_{cm^2}$)
Co-60	-	0.6
6 MV	0.670	1.3
10 MV	0.732	1.7
15 MV	0.765	1.9
24 MV	0.805	2.1

- **Partial occlusion of the photon source by the collimating devices**

The second problem is due to the effect of primary source occlusion when the field size is comparable to or smaller than the size of primary photon source. When the collimators are adjusted to be smaller than the size of primary photon source, the penumbra regions will overlap and lead into a significant deviation with the original treatment plan. The effect of partial source occlusion also influences the particle spectrum and creates a source of steep local absorbed dose gradients which can contribute to the large effect on the detector response. As can be seen in Figure 2.2, when the field size is large enough without any occlusion, the FWHM of dose profiles exhibits similar field size to the actual field size setting. Once the field size is occluded to the similar distance of maximum secondary electrons, the penumbra from opposing edges starts to overlap and produces a small deviation between FWHM and actual field size setting. Eventually, when the field size becomes extremely smaller than the range of secondary electrons, the FWHM of dose profiles turns to be greater than the actual field size setting. [3]
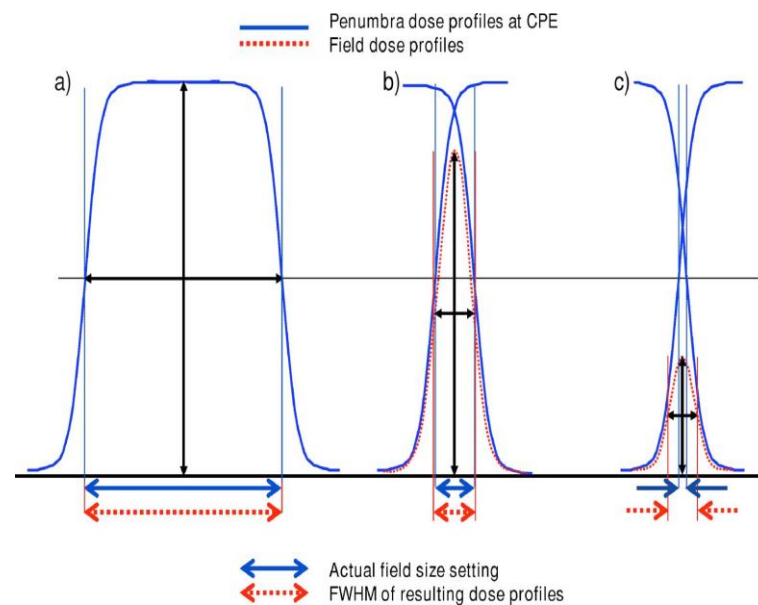
Figure 2.2 Partial occlusion of the primary photon source in small field.

The absence of LCPE along with the occlusion of primary photon source are responsible to produce a sharp drop in small field output. This drop is more pronounced when the beam energy increases or the density of material decreases. [4]

- **Detector related conditions**

The last problem is associated to the selection of detectors. Problems such as the volume averaging and perturbation effect of detectors are the major concern in small field. Farmer chamber is not suitable anymore since it possess an active volume wider than the radiation field which resulting into the volume averaging effect. [8] The volume averaging effect is related to the detector produces a signal that is proportional to the mean absorbed dose over its sensitive volume. This signal is influenced by the homogeneity of absorbed dose over its sensitive volume. [18] The second problem is perturbation effect of the charged particle fluence. This factor takes into account the difference between material composing the detector and the medium of measurement. In the presence of large dose gradients and absence of LCPE, the fluence perturbation turns to be large.[4] When the external

edge of detector volume is at a distance from the field edge smaller than the r_{lcpe} in medium, the small field condition starts to exist. As a solution suggested by IAEA/AAPM TRS 483, the beam half width or beam radius has to be at least as large as the range of charged particle equilibrium plus the half size of the external volume of detector. Moreover, the field output correction factors should be used to address the determination of field output factors in small field. The new protocol for small field dosimetry has listed the correction factors depending on the beam energy, types of equipments (Cyber Knife, Gamma Knife, Linear Accelerator, and TomoTherapy), and types of recommended detectors.

2.1.2 Commissioning of Treatment Planning System (TPS)

TPS is one of the essential parts when utilizing the external beam radiotherapy machine. The accuracy of dose calculation is undoubtedly important to guarantee the safety of treatment delivery as well as to avoid any poor radiation outcome. TPS is employed to set the beam arrangements, select the energies, field sizes, fluence patterns, and beam modifiers to optimize the dose distributions. Overall, the commissioning procedure involves three important steps: (1) beam data acquisition, (2) beam modelling, and (3) beam verification. [19] Commissioning procedure should be performed by a Qualified Medical Physicist. Attention should be made when identifying any required equipments such as the detectors and phantoms for measurement. For beam data acqusition, there are several beam characteristics which have to be measured such as percentage depth doses (PDDs), beam profiles, and field output factors. For PDDs and beam profiles, beam data should be collected from 0 cm depth until approximately 40 cm depth in various field sizes range from 1x1 cm^2 to 40x40 cm^2 field size. Reference detector is strongly advised to use in order to reduce beam output fluctuations. For field output factors, measurement is recommended to perfom at the reference depth of 10 cm. To collect the output factors in small field, the use of small volume detector is needed in order to minimize volume averaging effects. The results should be compared to the output at larger field size measured using larger volume chamber. [20]

Once beam commissioning has been completed, additional TPS check procedure such as dose volume histogram (DVH) calculation, effective depth calculation, and CT number consistency should be made to ensure the consistency of dose calculation. [21]

2.1.3 Implementation of small field concept in Linear Accelerator

Technological advancement in small field has been incorporated to the Linear Accelerator such as IMRT technique and VMAT technique. Additionally, special techniques such as SRS, SRT, and SBRT also rely on small field concept. IMRT technique uses an approach for obtaining the highly conformal dose distribution using multiple beamlets from several different angles. The field size is often designated small with the use of multi leaf collimator (MLC). IMRT is suitable for several indications such as head and neck cancer, pituitary tumors, and spinal cord tumors. On the other hand, SRS, SRT, and SBRT techniques are based on stereotactic concept. Stereotactic from its origin comes from Greek words, *stereo and taxis,* is a method which defines a point in patient's body by using an external three-dimensional coordinate system which is rigidly attached to the patient. For the terms "*stereotactic radiosurgery*", it was originally coined by Professor Lars Leksell, a neurosurgeon from Karolinska Institute, Sweden. [22] The terms between SRS and SRT is quite similar where both advanced radiotherapy techniques are able to deliver high radiation dose to small focus area. However, SRS refers to a single session of treatment delivery while SRT is more likely to be delivered more than single fraction. SRS is commonly used to treat brain lesions such as brain metastasis, meningioma, acoustic neurinoma, trigeminal neuralgia, and astrocytoma. Linac based SRS is typically entangled with VMAT technique. [23] Unlike 3D-CRT and IMRT which operate in the static conditions, VMAT operates dynamically with the gantry rotation and creates more conformal radiation dose to the tumor compared to 3D-CRT and IMRT techniques. Meanwhile, the SBRT technique is generally used to treat lung cancer. SBRT employs a coordinate system to precisely locate the tumor inside the lung region and hence could potentially minimize the radiation dose to surrounding healthy tissues. [24]

2.1.4 Monitor Unit

Monitor Unit could be defined as a measure of radiation "beam-on" time used for medical Linear Accelerators. By convention, one monitor unit equals to 1 cGy of absorbed dose in water under the specific calibration. [25] According to AAPM Task Group 71, calculation of MU for photon beams in 3D-CRT technique could be made by using either TPR (isocentric) method or PDD (nonisocentric) method. The following formulas are used to calculate MU [13] :

- **Isocentric Method**

$$MU = \frac{D}{D_o'.S_c(r_c).S_p(r_d).TPR(d,r_d).WF(d,r_d,x).TF.OAR(d,x).(\frac{SSD_0+d_0}{SPD})^2} \tag{2.2}$$

In case where the dose is calculated at the isocenter point, the formula above could be simplified to :

$$MU = \frac{D}{D_o'.S_c(r_c).S_p(r_d).TPR(d,r_d).WF(d,r_d,x).TF.(\frac{SSD_0+d_0}{SAD})^2} \tag{2.3}$$

- **Non isocentric Method**

$$MU = \frac{D.100\%}{D_o'.S_c(r_c).S_p(r_d).PDD_N(d,r,SSD).WF(d,r_d,x).TF.OAR(d,x).(\frac{SSD_0+d_0}{SSD+d_0})^2} \tag{2.4}$$

whereas,

D = The absorbed dose at the point of interest from the individual field under calculation.

D_o' = The dose rate or dose per MU under normalization conditions.

$S_c(r_c)$ = The ratio of the output in air for a given field size to that for reference field size.

$S_p(r_d)$ = The ratio of the dose per MU at normalization depth for a given field size in water phantom to that of the reference field size for the same incident energy fluence.

$TPR(d,r_d)$ = Tissue Phantom Ratio. The ratio of dose rate at any depth to dose rate at the normalization depth for a given field size in phantom.

$WF(d, r_d, x)$ = Wedge Factor. The ratio of dose rate at point of calculation using wedge to the similar field without the use of wedge.

TF = Tray Factor. The ratio of central axis dose rate for any field size with and without a blocking tray.

SSD_o = Standard source to surface distance.

d_o = Normalization depth for photon and electron dosimetry.

SPD = Source to point distance.

$S_p(r_d)$ = Phantom scatter factor. The ratio of dose per MU at normalization depth for any field size in water phantom to the reference field size for the same incident energy fluence.

$PDD_N(d, r, SSD)$ = Normalized percent depth dose.

$OAR(d, x)$ = Off-axis-ratio.

SSD = Source to surface distance.

On the other hand, for advanced techniques such as intensity modulated arc therapy (IMRT) and volumetric modulated arc therapy (VMAT), calculation of MU depends on several parameters attributed to the treatment planning system particularly the algorithm. In addition, the number of treatment fields as well as MLC movement could affect the calculated MU for each plan. [26]

2.1.5 Acuros XB algorithm

The Acuros XB algorithm is a computation algorithm in Eclipse™ treatment planning system. Unlike its predecessor, AAA which is based on convolution method, the AXB uses deterministic method of discretized cross sections to solve the linear Boltzman transport equation. Additionally, AXB takes into account the chemical composition of each material in the volume during radiation transport in medium. Therefore, drawback of AAA to compute the dose in the non-homogeneous medium could be solved by using AXB. [27] Furthermore, study has demonstrated a good agreement between AXB and Monte Carlo simulation.

In details, the AXB algorithm consists of four main steps which could be elaborated as follows [28] :

a. Transportation of source model fluence into the patient.

b. Calculation of scattered photon fluence in the patient.

c. Calculation of scattered electron fluence in the patient.

d. Dose calculation.

Steps (a) through (c) are performed to compute the electron fluence in every voxel of patient. Once the energy dependent of electron fluence is solved, the desired dose quantity is calculated following the Step (d). Step (a) is the only step which performed multiple times for each beam. Steps (b) through (d) are performed in a single time regardless of the number of beams. In VMAT technique, each beam will have a large number of orientations. For step (a), the machine sources are treated as external sources and ray tracing is performed to calculate the uncollated photon along with the distribution of electron fluence in patient. For step (b) and (c), the AXB discretizes in space, angle, and energy to iteratively solves the LBTE. Lastly, the dose in any voxel is obtained through implementing an energy dependent fluence at that voxel.

2.1.6 Field output factors

The definition of field output factors is a ratio of the absorbed dose to water in the clinical field (f_{clin}) for a given beam quality (Q_{clin}) to the absorbed dose to water in the machine specific reference field (f_{msr}) with the corresponding beam quality (Q_{msr}) as can be seen in equation 2.5.

$$\Omega_{\Omega_{clin}\Omega_{ref}}^{f_{clin}f_{ref}} = \frac{D_{w,Qclin}^{fclin}}{D_{w,Qmsr}^{fmsr}} \tag{2.5}$$

The formula above, however, could not be assumed proportional to the ratio between detector reading in the clinical field (M_{Qclin}^{fclin}) and detector reading in machine specific reference field (M_{Qmsr}^{fmsr}). The correction factors ($k_{\Omega_{clin}\Omega_{ref}}^{f_{clin}f_{ref}}$) must be applied to the ratio of detector reading as given in equation 2.6. The determination of small field output factors without applying correction factors has been reported as the main reason of an accidental overdosage in treatment delivery to patients. [29]

$$\Omega_{\Omega_{clin}\Omega_{ref}}^{f_{clin}f_{ref}} = \frac{M_{Qclin}^{f_{clin}}}{M_{Qmsr}^{f_{msr}}} k_{\Omega_{clin}\Omega_{ref}}^{f_{clin}f_{ref}} \tag{2.6}$$

The terms, f_{msr}, is introduced as the machine specific reference field for equipments that unable to establish the conventional reference field size. For instance, the machine specific reference field for Cyber Knife is 6 cm diameter collimator, for Gamma Knife is 16 mm or 18 mm diameter collimator depending on its type, and for TomoTherapy is 5 cm x 20 cm. It is advisable that the machine specific reference field should be as close as possible to the 10x10 cm² field size. The terms clinical field size (f_{clin}) denotes the clinical radiation field for which the absorbed dose to water needs to be determined. [4] [12]

Following the previous equation, effort to determine the field output correction factors ($k_{\Omega_{clin}\Omega_{ref}}^{f_{clin}f_{ref}}$) has been conducted by several investigators for various types of the detectors. [10] [30] The field output correction factors can be determined using an experimental measurement or Monte Carlo from equation 2.7 as given below :

$$k_{\Omega_{clin}\Omega_{ref}}^{f_{clin}f_{ref}} = \frac{D_{w,Qclin}^{f_{clin}}/M_{w,Qclin}^{f_{clin}}}{D_{w,Qmsr}^{f_{msr}}/M_{w,Qmsr}^{f_{msr}}} \tag{2.7}$$

IAEA/AAPM TRS 483 has tabulated the field output correction factors as a function of equivalent square field size for radiotherapy equipments based on small field concept such as Cyber Knife, Gamma Knife, TomoTherapy, and for 6 MV and 10 MV Linac WFF & FFF. The correction factors are available for large set of recommended detectors for small field dosimetry.

2.1.7 Radiation dosimeters

There are many kind of radiation dosimeters that have been observed for small field dosimetry such as ionization chambers and diode detectors. Radiation dosimeters are instruments that measure or evaluate, either directly or indirectly, the quantities of exposure, kerma, absorbed dose, dose rate and other related quantities of ionizing radiation. Radiation dosimeter along with its reader is referred to as the

dosimetry system. [31] For small field dosimetry, selection of appropriate detectors should be considered following several general characteristics from the current protocol. Those involve detector stability, dose linearity, energy dependence, spatial resolution, size of collecting volume, orientation of detector, and background signal. Interested readers are suggested to see the protocol for further details. [4]

In this research, explanation will be emphasized to the ionization chamber and diode detector.

- **Ionization chamber**

Ionization chamber is oftenly used for radiotherapy dosimetry since it provides excellent stability and linear response to absorbed dose. Ionization chamber consists of a gas filled cavity surrounded by conductive outer wall with central collecting electrode. The wall and central collecting electrode are separated with a high quality of insulator in order to reduce the leakage current when a polarizing voltage is applied to the chamber. The sensitive medium in ionization chamber is air at atmospheric pressure with density around 700 times lesser than water. Ionization chamber requires a sufficient voltage to avoid recombination ion.[4] Another advantageous of ionization chamber are dose rate independence, less energy dependence, good stability, high sensitivity, robust, and low leakage effect. Most of ionization chambers are also impervious to water. This enables the measurement to be performed directly in water phantom.

Especially for thimble ionization chamber, TRS 483 gives recommendation to employ this type of detector for clinical reference dosimetry in machine specific reference field (msr) in water or solid phantoms. Construction of ionization chamber, however, should be made as homogeneous as possible since the difference of materials composing the chamber could affect the energy response of ionization chamber. Furthermore, the air cavity is recommended to be sealed in order to keep the air equilibrates rapidly with the temperature and pressure.[4]

- **Diode detector**

Diode detector is a type of detector which uses the main component of semiconductor (*Silicon*) material. Diode detector consists of a *p-n* junction which is

created by taking the *n*-type or *p*-type of silicon materials and counter-doping the surface to produce the opposite type material. Diode detector is more sensitive and smaller in size compared to the ionization chamber. Unlike the ionization chamber, the diode detector requires no pressure correction and no high voltage to operate. However, the temperature correction is still required and ageing effect of silicon diode should be considered. The angular dependence and energy dependence of diode detector also add other pitfalls when employing diode detectors. [9] [14]

In small field dosimetry, two types of diode detectors are commonly used. They are shielded and unshielded diode. Shielded diode is made from p-silicon diode while the unshielded diode is developed from the n-silicon diode. One of the main factors to distinguish both diode detectors is the use of shielding material. For the shielded diode, metallic shielding with high atomic number is employed in order to eliminate the scattered photons of low energy which is attributed to the photoelectric effect after interaction with Silicon material. [32] Unlike the shielded diode, the unshielded diode contains no metallic shielding and hence able to minimize the effect from scattered radiation. However, the unshielded diode is not suitable to measure the output factors in broad fields as it may introduce an over-response due to the interaction with low energy scattered photon beams in large fields. [9]

2.2 Review of related literatures

Kerracher et al. [33] assessed the use of several dosimeters for sterotactic beam data acquisition: Scanditronix shielded diode, Scanditronix unshielded diode, Scanditronix unshielded mini diode, PTW ion chamber 0.125 cc, PTW Pinpoint ion chamber 0.015 cc, PTW Markus parallel plate 0.05 cc, and Kodak X-Omat film. Measurements were carried out on ABB CH6 6 MV Linear Accelerator dedicated for stereotactic treatments via radionics system. Beam data acquisition was made such as measurement of percent depth doses, off-axis-ratio, and relative output factors for circular fields in 40-12.5 mm diameter range. Some important findings from their study were all dosimeters yielded well agreement in PDD measurement for all circular collimators. For off-axis-ratio, ion chamber demonstrated broader penumbra

than measurement using diode detectors. For small field output factors, a large deviation was pronounced with decreasing the field size. The shielded diode produced higher output factors and all ion chambers began to underestimate the output due to the volume averaging effect. Results from unshielded diode were completely different with shielded diode where all unshielded diode consistently exhibited lower output. They summarized their work by advising the use of unshielded diode along with ion chamber and other dosimeter such as film to accurately obtain the stereotactic beam data.

Alfonso et al. [12] proposed a formalism for reference dosimetry of small and static fields. This new formalism introduced the concept of machine specific reference field (f_{msr}) of a given quality beam (Q_{msr}). In addition, the formula could be extended to calculate the dose to water for a clinical field size, $D_{w,Q_{clin}}^{f_{clin}}$ by using following formula:

$$D_{w,Q_{clin}}^{f_{clin}} = D_{w,Q_{msr}}^{f_{msr}} \Omega_{Q_{clin},Q_{msr}}^{f_{clin},f_{msr}} \tag{2.8}$$

This equation formulated the field output factors $(\Omega_{Q_{clin}Q_{msr}}^{f_{clin}f_{msr}})$ as the ratio of the detector reading in the clinical field $(M_{Q_{clin}}^{f_{clin}})$ to the detector reading in the machine reference field $(M_{Q_{msr}}^{f_{msr}})$ and applied the output correction factors $(k_{Q_{clin}Q_{msr}}^{f_{clin}f_{msr}})$ as previously described in equation 2.6.

Benmakhlouf et al. [30] published the output correction factors $(k_{Q_{clin},Q_{msr}}^{f_{clin},f_{msr}})$ for nine different detectors determined by using PENELOPE Monte Carlo simulation. They were PTW T60016 shielded diode, PTW T60017 unshielded diode, PTW T31016 ionization chamber, PTW T31018 micro liquid ionization chamber (LIC), PTW T60003 diamond dosimeter, IBA PFD shielded diode, IBA EFD unshielded diode, IBA SFD unshielded diode, and IBA CC01 ionization chamber. Field sizes were set from the largest 10x10 cm² to the smallest field size of 0.5x0.5 cm² in Varian Clinac iX 6MV. Their study showed the result for the LIC (PTW T31018) and for diamond dosimeter (PTW T60003) yielded correction factors within 1% for the smallest field size. For the air filled ionization chambers, the corrections were up to 5%-15% for the smallest

field size and the main problem affecting the output correction factor was volume averaging effect. The air filled ionization chamber was not suitable to determine output factors for field sizes less than 2x2 cm². For silicon diodes, the correction factors were of the order from -1% to -9% for the smallest field sizes. The other interesting conclusion in this research was the small active dimension of dosimeters was not always considered as the important requirement to select dosimeters for small fields dosimetry. This conclusion was derived from the calculated correction factors for some silicon diodes with small dimensions and exceeded those for intermediate-sized silicon diodes.

Garcia-Garduno et al. [34] observed the impact of several dosimeters on the calculated dose distribution in SRS. They employed six different dosimeters: SFD dosimeter, SRS dosimeter, silicon diode E, CC01 ionization chamber, and two types of radiochromic films: EBT and EBT2. They chose EBT radiochromic film as the reference dosimeter since they have proved an excellent agreement between EBT film and Monte Carlo in their previous study in 2010. This study was performed on a 6 MV Novalis Linear Accelerator. The field sizes were set by using circular collimators with various diameters. In the beginning, they compared the dosimetric parameters such as TSF, TPR, and OAR acquired from each dosimeter. Secondly, the commissioning dataset were incorporated to iPlan version 4.1. In summary, they found all dosimeters produced similar commissioning dataset for TPS dose calculations and satisfied the gamma index criteria and DVH. However, the result of this study only validated the dose distribution and did not pay attention to the calculated MU.

CHAPTER III

RESEARCH METHODOLOGY

3.1 Research design

This research is an observational descriptive study based on the retrospective study.

3.2 Research design model

This research was divided into three major steps. The first step was measurement of percentage depth doses (PDDs) and beam profiles using CC01, PFD, EFD, and EDGE, followed by determination of field output factors using CC01, PFD, and EFD. The second step was TPS commissioning in Eclipse™, and the last step was observation of calculated MU among commissioning datasets. Figure 3.1 displays the diagram of the whole steps in this research.

```
┌─────────────────────────────────────────────────────────────────────────┐
│ Measurement of PDDs, Beam Profiles, and Field output factors using CC01,  │
│ PFD, and EFD                                                              │
└─────────────────────────────────────────────────────────────────────────┘
```

```
┌──────────────────────┐                          ┌──────────────────────┐
│ Apply field output   │                          │ Omit the use of      │
│ correction factors   │                          │ field output         │
│ according to         │                          │ correction factors   │
│ IAEA/AAPM TRS 483     │                          └──────────────────────┘
└──────────────────────┘

┌──────────────────────┐                          ┌──────────────────────┐
│ Corrected field      │                          │ Average uncorrected  │
│ output factors from  │                          │ field output factors │
│ each detector        │                          │ from three detectors │
└──────────────────────┘                          │ (CC01, PFD & EFD)    │
                                                   └──────────────────────┘
```

```
┌─────────────────────────────────────────────────────────────────────────┐
│ TPS Commissioning in Eclipse™ to create four beam commissioning datasets  │
└─────────────────────────────────────────────────────────────────────────┘
```

```
┌──────────────┐ ┌──────────────┐ ┌──────────────┐ ┌──────────────┐
│ Beam         │ │ Beam         │ │ Beam         │ │ Beam         │
│ Commissioning│ │ Commissioning│ │ Commissioning│ │ Commissioning│
│ from measured│ │ from measured│ │ from measured│ │ from average │
│ PDDs, Beam   │ │ PDDs, Beam   │ │ PDDs, Beam   │ │ uncorrected  │
│ Profiles     │ │ Profiles     │ │ Profiles     │ │ FOF from     │
│ (1x1cm² to   │ │ (1x1cm² to   │ │ (1x1cm² to   │ │ three        │
│ 10x10cm²),   │ │ 10x10cm²),   │ │ 10x10cm²),   │ │ detectors    │
│ and corrected│ │ and corrected│ │ and corrected│ │ (CC01, PFD & │
│ FOF from CC01│ │ FOF from PFD │ │ FOF from EFD │ │ EFD)         │
└──────────────┘ └──────────────┘ └──────────────┘ └──────────────┘
```

```
┌─────────────────────────────────────────────────────────────────────────┐
│ PDDs and Beam Profiles from 12x12cm² to 40x40 cm² field size measured     │
│ using CC13 ionization chamber were already available in the beam          │
│ commissioning datasets                                                    │
└─────────────────────────────────────────────────────────────────────────┘
```

```
┌─────────────────────────────────────────────────────────────────────────┐
│ Comparison of calculated MU in symmetric fields, IMRT-SRS plans, and      │
│ VMAT-SRS plans                                                            │
└─────────────────────────────────────────────────────────────────────────┘
```

Figure 3.1 Diagram of research design model.

3.3 Conceptual framework

Validation of MU in this study was affected by several factors as described in Figure 3.2.
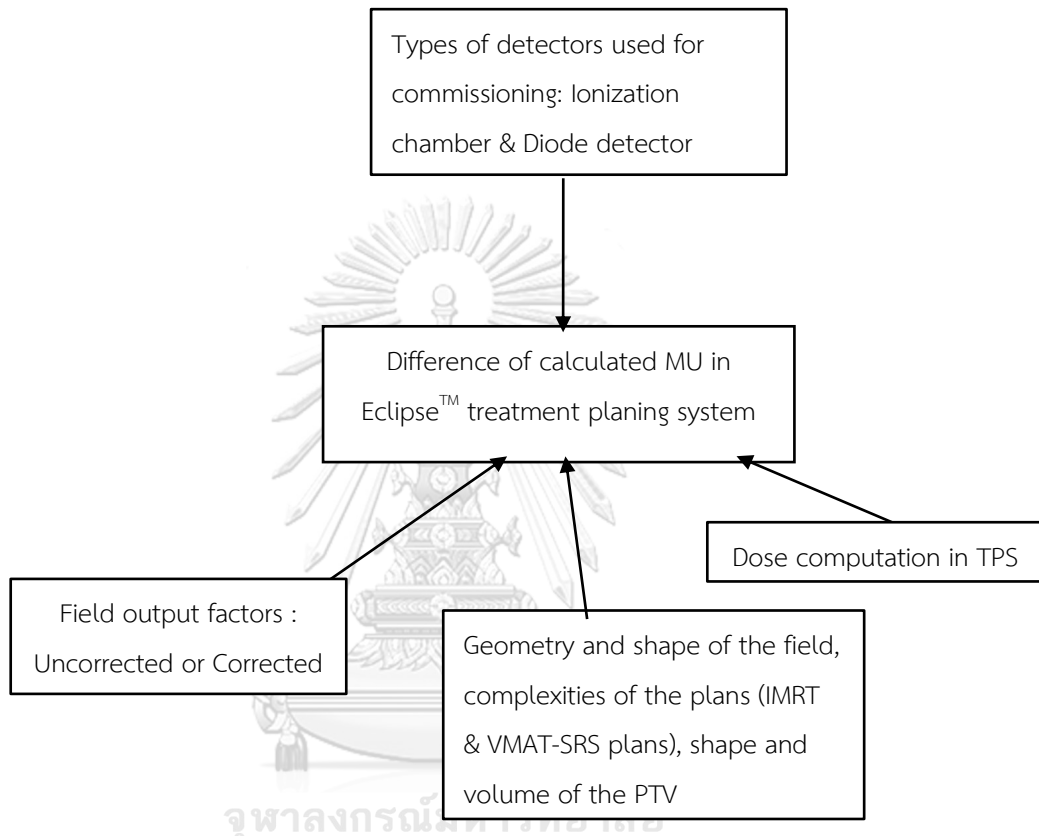
Figure 3.2 Conceptual framework.

3.4 Research question

What are the calculated MU differences in the symmetric fields, IMRT-SRS plans, and VMAT-SRS plans between beam commissioning dataset where the correction factors $(k_{Q_{clin}Q_{msr}}^{f_{clin}f_{msr}})$ based on IAEA/AAPM TRS 483 are implemented and beam commissioning dataset where the correction factors are not implemented ?

3.5 Research objective

To determine the differences of calculated MU in symmetric fields, IMRT-SRS plans, and VMAT-SRS plans between beam commissioning dataset where the correction factors ($k_{Q_{clin}Q_{msr}}^{f_{clin}f_{msr}}$) based on IAEA/AAPM TRS 483 are implemented and beam commissioning dataset where the correction factors are not implemented.

3.6 Materials

The materials used in this study were supplied from the Division of Radiation Oncology, Department of Radiology, Faculty of Medicine, Chulalongkorn University.

3.6.1 Linear Accelerator

This research employed Varian TrueBeam™ Linear Accelerator (Varian Medical Systems, Palo Alto, CA, USA) as displayed in Figure 3.3. The Varian TrueBeam™ Linear Accelerator provides all forms of advanced external beam radiotherapy including IGRT as well as IGRS, IMRT, SBRT, and VMAT techniques. Varian TrueBeam™ Linear Accelerator also provides two photon energies: 6 MV and 10 MV. Both energies are available in flattened and unflattened photon beams. The electron beams are also provided in various energies: 6, 9, 12, 15, 18, and 22 MeV. The Varian TrueBeam™ Linear Accelerator is also equipped with 120 leaves of MLC. For this work, the 6 MV with flattenning filter (flattened) photon beams was used.

Figure 3.3 Varian TrueBeam™ Linear Accelerator.

3.6.2 Eclipse™ treatment planning system

Eclipse™ treatment planning system (Varian Medical System, Palo Alto, CA, USA) version 11.0.31 as displayed in Figure 3.4 was used. Eclipse™ is an integrated and comprehensive treatment planning system to support the external beam therapy such as 3D-CRT, IMRT, VMAT, brachytherapy, electron, and proton therapy. Eclipse™ provides two photon dose calculation algorithms: AAA and AXB algorithm.

Figure 3.4 Eclipse™ treatment planning system.

3.6.3 Ionization chamber

IBA CC01 ionization chamber (IBA Dosimetry, Nuremberg, Germany) as shown in Figure 3.5 possess an active volume of 0.01 cm³ with an inner electrode made of steel. The diameter and length of the inner electrode are 0.35 mm and 2.8 mm, respectively. The outer part of this detector is fabricated from Shonka plastic with 2 mm inner diameter and 0.5 mm wall thickness. Table 3.1 lists the overall specification of this chamber.

Figure 3.5 IBA CC01 microionization chamber.

Table 3.1 Specification of IBA CC01 ionization chamber.

Detector	Cavity Volume (cm³)	Cavity Length (mm)	Wall Material	Wall Thickness(g/cm^2)	Central Electrode material
IBA CC01	0.01	3.6	C-552	0.088	Steel

3.6.4 Diode detector

Three diode detectors were employed in this study. They were IBA PFD (IBA Dosimetry, Nuremberg, Germany), IBA EFD (IBA Dosimetry, Nuremberg, Germany), and Sun Nuclear EDGE (Sun Nuclear Corporation, Melbourne, FL). The IBA PFD and IBA EFD were utilized to determine the field output factors as well as to measure PDDs and Profiles. Meanwhile, the EDGE detector was only appointed to measure PDDs and Profiles. The characteristics of all diode detectors are tabulated in Table 3.2. Figure 3.6 and 3.7 display the picture of all diode detectors used in this research.

a   b
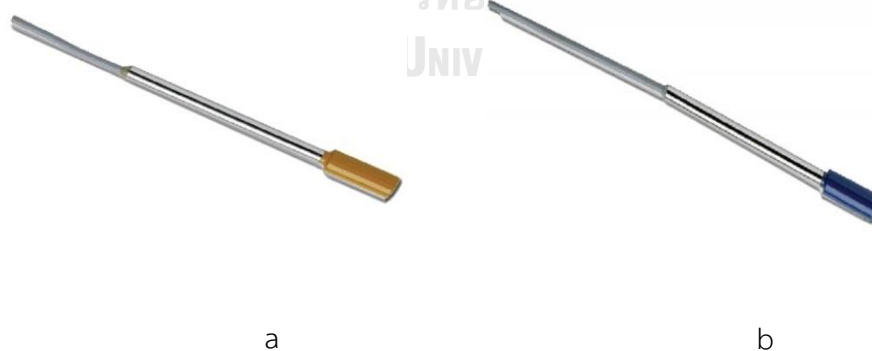
Figure 3.6 IBA PFD (a) and IBA EFD (b).

Figure 3.7 Sun Nuclear EDGE Detector.

Table 3.2 Specification of diode detectors used in this research.

Detector	Sensitive Volume (cm³)	Diameter of side length of sensitive area (mm)	Geometric form of sensitive area	Thickness of sensitive area (mm)	Possess Shielding material (Yes/No)
IBA PFD3G	0.00019	2	Disc	0.06	Yes
IBA EFD3G	0.00019	2	Disc	0.06	No
Sun Nuclear EDGE	0.000019	0.8	Square	0.03	Yes

3.6.5 Beam scanning water phantom

The beam scanning water phantom used in this work was IBA blue water phantom (IBA Dosimetry, Nuremberg, Germany) as presented in Figure 3.8. This phantom is made from acrylic plastic (Perspex). The positional accuracy and positional resolution of this water phantom is ± 0.1 mm and operated through the OmniPro-Accept software. The dimension of this phantom is 48 cm x 48 cm x 41 cm.

Figure 3.8 IBA blue water phantom.

3.6.6 Electrometer

To measure the collection charge during the output measurement, the Dose1 Electrometer (Wellhofer Dosimetry, Schwarzenbruck, Germany) as shown in Figure 3.9 was connected to each detector. This electrometer is able to measure the electrical charge in the range from 40 pC to 1.0 C at the resolution of 0.1 pC. The ion collection charge will be visualized clearly in the digital number. This type of electrometer is convenient for the use of ionization chambers, diode detectors, as well as diamond detectors.

Figure 3. 9 Dose 1 electrometer.

3.7 Methods

3.7.1 Percentage depth doses

The following steps are the procedures to scan the percentage depth doses:

1. The SSD was set into 100 cm.

2. The depth dose ionization curves were scanned in IBA blue water phantom using all detectors. For measurement using CC01, the effective point of measurement was taken into account following the recommendation from TRS 398 where it was positioned towards the surface at a distance equal to 0.6 r_{cyl} (internal radius of cylindrical ionization chamber). [35] For measurement using PFD, EFD, and EDGE, the effective point of measurement was at its surface and orientated directly to the direction of beam.

3. The depth dose ionization curves were scanned using all detectors subsequently from 10x10 cm², 6x6 cm², 4x4 cm², 3x3 cm², 2x2 cm², 1.5x1.5 cm², and 1x1 cm² field size. The scanning depth was started from 400 mm to 0 mm.

4. After scanning, smoothing procedure was made using Omni-pro Accept software.

5. The percentage depth doses from each detector were recorded.

3.7.2 Beam profiles

For beam profiles, measurement was made in the cross-plane direction. The following steps are the procedures to scan the beam profiles:

1. The SSD was set into 100 cm.

2. The beam profiles were scanned using all detectors subsequently in IBA blue water phantom from 10x10 cm², 6x6 cm², 4x4 cm², 3x3 cm², 2x2 cm², 1.5x1.5 cm², and 1x1 cm² field size at the depth of maximum dose (d_{max}).

3. Smoothing was made using Omni-pro Accept software.

4. The beam profiles from each detector were recorded.

3.7.3 Equivalent square field size

The following steps are the procedures to compute the equivalent square field size according to IAEA/AAPM TRS 483. Measurement was performed using only Sun Nuclear EDGE detector.

1. The SSD was set into 100 cm.

2. The beam profiles were scanned in IBA blue water phantom from 10x10 cm², 6x6 cm², 4x4 cm², 3x3 cm², 2x2 cm², 1.5x1.5 cm², and 1x1 cm² field size at 10 cm reference depth. Measurement was made in the cross-plane and in-plane direction.

3. Smoothing was made using Omni-pro Accept software.

4. The dosimetric field width at 50% of relative dose (FWHM) from the cross-plane and in-plane direction were recorded.

5. Using the measured data from step 2, the equivalent square field size was calculated following equation 3.1:

$$S_{clin} = \sqrt{A\,B} \qquad\qquad\qquad (3.1)$$

where the A and B were the dosimetric field width of cross-plane and in-plane direction defined at the 50% of relative dose, respectively. The equivalent square field size of each geometrical field was assigned through linear interpolation method to derive the field output correction factors based on Table 3.3.

3.7.4 Field output factors

The determination of FOF was classified into two groups. The first group was the uncorrected FOF and the second group was the corrected FOF. The procedures to determine both groups are explained below:

- **Uncorrected FOF**

1. The SSD and reference depth of measurement were adjusted to 100 cm and 10 cm, respectively.

2. The output was measured at the clinical field size and at machine specific reference field size. The detector reading in the clinical field size $(M_{Q_{clin}}^{f_{clin}})$ was collected at 6x6 cm², 4x4 cm², 3x3 cm², 2x2 cm², 1.5x1.5 cm², and 1x1 cm²

field size. Meanwhile, the detector reading at machine specific reference field size (M_{Qmsr}^{fmsr}) was collected at 10x10 cm² field size. Three detectors consist of CC01, PFD, and EFD were utilized subsequently. Afterward, the field output factors for all field sizes were computed as the ratio between detector reading in the clinical field size (M_{Qclin}^{fclin}) and detector reading at machine specific reference field size (M_{Qmsr}^{fmsr}).

3. The average uncorrected FOF was obtained after calculating the average field output factors from three detectors.

- **Corrected FOF**

1. The SSD and reference depth of measurement were adjusted to 100 cm and 10 cm, respectively.

2. The output was measured at the clinical field size and at machine specific reference field size using CC01, PFD, and EFD. The detector reading at clinical field size (M_{Qclin}^{fclin}) was collected at 6x6 cm², 4x4 cm², 3x3 cm², 2x2 cm², 1.5x1.5 cm², and 1x1 cm² field size. Meanwhile, the detector reading in machine specific reference field size (M_{Qmsr}^{fmsr}) was collected at 10x10 cm² field size.

3. The field output correction factors ($k_{QclinQmsr}^{fclinfmsr}$) as shown in Table 3.3 were applied to the ratio of detector reading for CC01, PFD, and EFD as given in equation 3.2. It should be noted that the correction factors were derived based on the equivalent square field size as previously explained. Therefore, the linear interpolation based on equivalent square field size was made prior to the use of field output correction factors for each detector.

$$\Omega_{Q_{clin}Q_{msr}}^{f_{clin}f_{msr}} = \frac{M_{Q_{clin}}^{f_{clin}}}{M_{Q_{msr}}^{f_{msr}}} \, k_{Q_{clin}Q_{msr}}^{f_{clin}f_{msr}} \tag{3.2}$$

4. The corrected FOF from each detector was recorded as a function of geometrical field size and equivalent square field size.

Table 3.3 Field output correction factors for 6 MV flattened photon beams as a function of equivalent square field size based on IAEA/AAPM TRS 483.

Detector	Equivalent square field size (S_{clin}) / (cm^2)								
	8.0	6.0	4.0	3.0	2.5	2.0	1.5	1.2	1.0
IBA CC01	1.002	1.004	1.007	1.008	1.008	1.009	1.011	1.013	1.018
IBA PFD3G	1.000	1.000	0.998	0.995	0.992	0.986	0.976	0.968	0.961
IBA EFD3G	1.005	1.009	1.014	1.016	1.016	1.015	1.012	1.008	1.004

The difference between the corrected FOF from single detector ($(FOF)c$) and the average uncorrected FOF ($(FOF)u$) from three detectors was calculated following equation 3.3 below:

$$\%FOF\ Difference\ =\ \frac{(FOF)c-(FOF)u}{(FOF)u}\ x\ 100\%$$ (3.3)

3.7.5 TPS Commissioning in Eclipse™

After measurement of PDDs, Beam Profiles, and FOF were completed, all data were incorporated to the Eclipse™ version 11.0.31 for commissioning process. The measured small field output factors using three different detectors (CC01, PFD, and EFD) were added to the large field output factors (12x12 cm^2 to 40x40 cm^2 field size) which measured using CC13 ionization chamber. The small and large field output factors were smooth. The daisy chain correction method as shown in equation 3.4 was employed to link the field output factors between small and large fields. Total four commissioning datasets were generated. The AXB algorithm was selected as the dose calculation algorithm and a grid size of 0.125 cm was applied. Then, these four new commissioning datasets were used to calculate the MU in Eclipse™ for symmetric fields, IMRT-SRS plans, and VMAT-SRS plans. Figure 3.10 exhibits the screenshot of creating four beam commissioning datasets in our study. The "A" indicates the commissioning using average uncorrected FOF while the terms

"CC01_483", "PFD_483", and "EFD_483" indicate the commissioning using corrected CC01, corrected PFD, and corrected EFD, respectively.

$$OF_{Daisy\ chain} = [\frac{M_{clin}}{M_{int}}]_{det}\ x\ [\frac{M_{int}}{M_{ref}}]_{CC13} \tag{3.4}$$

Three variables: M_{clin}, $M_{int,}$ and M_{ref}, stand for detector reading for clinical field size, intermediate field size, and reference field size, respectively. In this work, detector reading at 6x6 cm^2 field size was appointed as detector reading at intermediate field size.
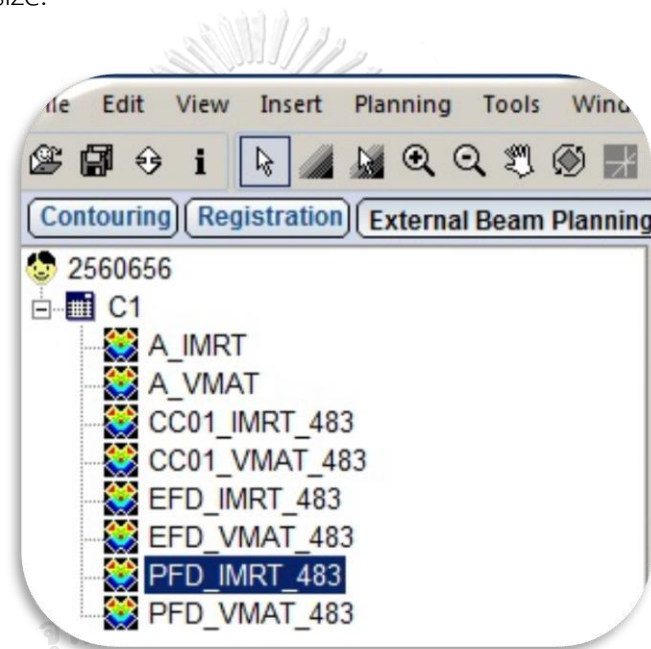
Figure 3.10 Four beam commissioning datasets in this work.

3.7.6 Validation of MU

Validation of MU was conducted in six symmetric fields started from 6x6 cm^2 to 1x1 cm^2 and 10 SRS cases of brain tumors treated using IMRT technique and VMAT technique. The steps are elaborated as follows:

- **Validation of MU in symmetric field sizes**

1. Virtual water phantom as illustrated in Figure 3.11 was created in Eclipse^{TM}.

2. Dose per fraction was prescribed to 100 cGy for single fraction. The SSD was set to 100 cm. All plans were normalized into 100% at the isocenter of field 1 in 10 cm depth.

3. Gantry rotation and collimator rotation were adjusted to 0 degree. No MLC and wedge were employed.

4. Both fields, X (cm) and Y (cm) were changed consecutively from 6 to 1 cm in order to segment the field size into 6x6 cm^2 until 1x1 cm^2 as depicted in Figure 3.12. Then, the plan was computed and the calculated MU from all square field sizes mentioned above were recorded.

5. Without changing any parameters, the calculated MU was continued to observe by altering the beam commissioning dataset from beam commissioning using corrected CC01, corrected PFD, corrected EFD, and average uncorrected FOF, continuously. Afterward, the plan was recomputed and the calculated MU was recorded according to each commissioning dataset.
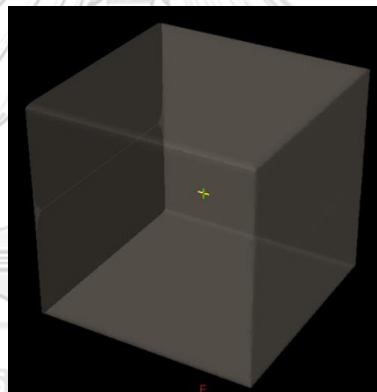

Figure 3. 11 Virtual water phantom in Eclipse™ treatment planning system.

a	b
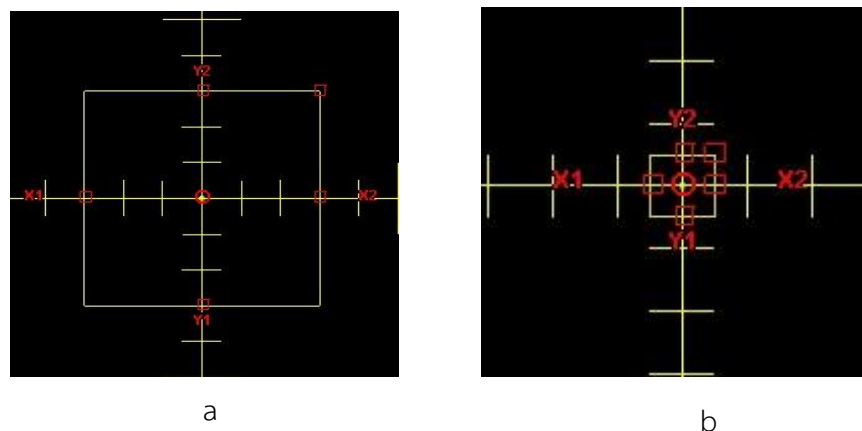
Figure 3. 12 Square field size of 6x6 cm^2 (a) and 1x1 cm^2 (b).

- **Validation of MU in IMRT-SRS and VMAT-SRS plans**

1. Validation was made in 10 SRS cases of brain tumors treated by using both techniques: IMRT and VMAT. For IMRT technique, nine fields were used and for VMAT technique, two-arcs of gantry rotation were utilized.

2. Similar to the validation in symmetric field sizes, all planning parameters were fixed. The optimization and dose constraints were also set similar. The only parameter changed was only the beam commissioning dataset.

3. The selection of ten cases was based on sample size determination in section 3.8. Table 3.4 summarizes the PTV of each case along with the prescribed dose.

   Shown in Figure 3.13, an example of SRS case treated using IMRT technique and VMAT technique.

a   b
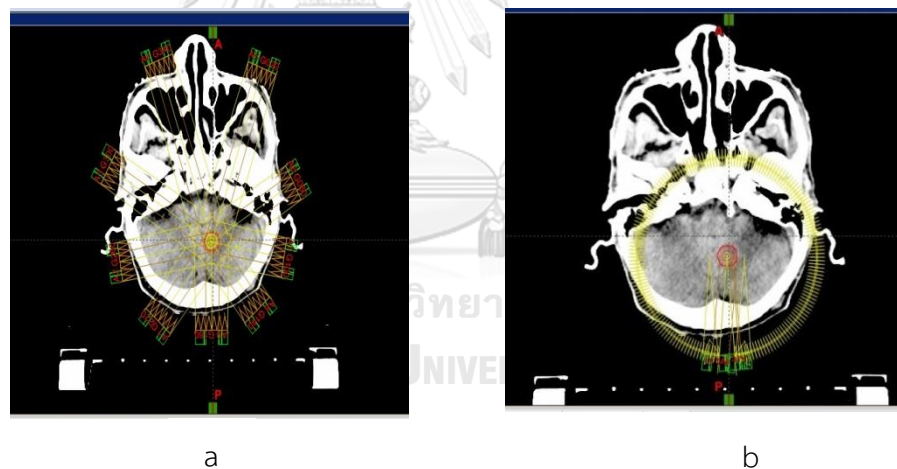
Figure 3.13 Case number 8 treated with IMRT technique (a) and VMAT technique (b).

The percentage MU difference was computed between the calculated MU from commissioning using single corrected detector ($(MU)_c$) and the calculated MU from commissioning using uncorrected FOF of three different detectors ($(MU)_u$) as mentioned in equation 3.5. For all cases, the prescribed doses were normalized to the planning target volume (PTV).

$$\%MU\ Difference\ =\ \frac{(MU)c-(MU)u}{(MU)u}\ x\ 100\%$$

$\hspace{10cm}$ (3.5)

3.8 Sample size determination

The sample size calculation to determine the number of IMRT-SRS and VMAT-SRS plans in this study was based on the following formula:

$$\left(\frac{(Z_{1-\alpha/2}+Z_{1-\beta})^2\sigma^2}{\Delta^2_{MDD}}\right) \tag{3.6}$$

whereas,

$Z_{1-\alpha/2}$=1.96 (95% of confidence level).

$Z_{1-\beta}$=(β = 0.1), therefore $Z_{0.9}$ =1.28.

σ=Standard Deviation ; according to the Rule of 6 = $\frac{Range\ of\ Value}{6}=\frac{4\%}{6}$ = 0,667% ; Assuming the range of value is 4%.

Minimum Detectable Difference (MDD), assuming the number of 1%.

By using this equation, we determined the sample size for 10 SRS cases of brain tumors treated by using IMRT technique as well as VMAT technique.

Table 3. 4 Summary of 10 brain SRS cases for MU validation in IMRT and VMAT techniques.

Case Number	PTV (cm³)	Prescribed Dose (Gy)
1	14.06	20
2	13.03	20
3	11.16	20
4	6.25	15
5	3.01	12.5
6	2.67	18
7	1.86	18
8	1.62	24
9	0.78	12.5
10	0.36	12.5

3.9 Outcome measurements

The outcome measurements of this study consist of the suitable dosimeter type for commissioning small field 6 MV flattened photon beams and the deviation of calculated MU between commissioning dataset after implementing the field output correction factors ($k_{Q_{clin}Q_{msr}}^{f_{clin}f_{msr}}$) according to IAEA/AAPM TRS 483 and commissioning dataset using average uncorrected field output factors from three different detectors.

3.10 Statistical analysis

Microsoft Excel 2016 was used to compute the statistical analysis in this study such as average, standard deviation, and percentage differences.

3.11 Data presentation format

Tables, graphs, and histograms were used to illustrate the data in this research.

3.12 Benefit of thesis

To obtain an information about the suitable dosimeter type for commissioning small field 6 MV flattened photon beams as well as the implication of field output correction factors based on IAEA/AAPM TRS 483.

3.13 Ethical consideration

The ethical issue of this study has been approved by Institutional Review Board, Faculty of Medicine, Chulalongkorn University, Bangkok, Thailand. The certificate of approval is given in Figure 3.14.

COE No. 031/2017

IRB No. 512/60

INSTITUTIONAL REVIEW BOARD

Faculty of Medicine, Chulalongkorn University

1873 Rama IV Road, Patumwan, Bangkok 10330, Thailand, Tel 662-256-4493

Certificate of Exemption

The Institutional Review Board of the Faculty of Medicine, Chulalongkorn University, Bangkok, Thailand, has exempted the following study in compliance with the International guidelines for human research protection as Declaration of Helsinki, The Belmont Report, CIOMS Guideline, International Conference on Harmonization in Good Clinical Practice (ICH-GCP) and 45CFR 46.101(b)

Study Title   : Monitor Unit(MU)Validation using various types of dosimeters for commissioning small
                        field in Eclipse™ Treatment Planning System

Principal Investigator   : Mr. Sammuel Mamesa

Study Center   : Department of Radiology, Faculty of Medicine, Chulalongkorn University.

Signature: ....   Signature: ....

(Emeritus Professor Tada Sueblinvong MD)   (Assistant Professor Prapapan Rajatapiti MD, PhD)

Chairperson   . Member and Secretary

The Institutional Review Board   The Institutional Review

Date of Exemption   : September 29, 2017

<u>Note</u> No continuing review report and final report when finish require

Figure 3. 14 Certificate of approval from institutional review board, Faculty of Medicine, Chulalongkorn University.

CHAPTER IV

RESULTS

4.1 Percentage depth doses and Beam profiles

4.1.1 Percentage depth doses

Shown in Figure 4.1, 4.2, 4.3, 4.4, 4.5, 4.6 and 4.7, the results of measured PDDs from 10x10 cm² to 1x1 cm² field size using CC01, PFD, EFD, and EDGE detector, respectively. The comparison of percent depth dose at 10 cm depth is given in Table 4.1. The percent SD started to increase as the field size decreased. Measured PDDs using diode detectors produced comparable outcomes, especially between PFD and EDGE. On the other hand, CC01 demonstrated slightly higher PDDs than diode detectors. This condition was more pronounced at deeper depth and smaller field size.

10x10 cm²

Figure 4.1 Percentage depth doses measured at 100 cm SSD, 10 cm depth, and 10x10 cm^2 field size using CC01, PFD, EFD, and EDGE.

6x6 cm²

Figure 4.2 Percentage depth doses measured at 100 cm SSD, 10 cm depth, and 6x6 cm^2 field size using CC01, PFD, EFD, and EDGE.

4x4 cm²

Figure 4.3 Percentage depth doses measured at 100 cm SSD, 10 cm depth, and 4x4 cm^2 field size using CC01, PFD, EFD, and EDGE.

3x3 cm²

Figure 4.4 Percentage depth doses measured at 100 cm SSD, 10 cm depth, and 3x3 cm^2 field size using CC01, PFD, EFD, and EDGE.

2x2 cm²

Figure 4.5 Percentage depth doses measured at 100 cm SSD, 10 cm depth, and 2x2 cm^2 field size using CC01, PFD, EFD, and EDGE.
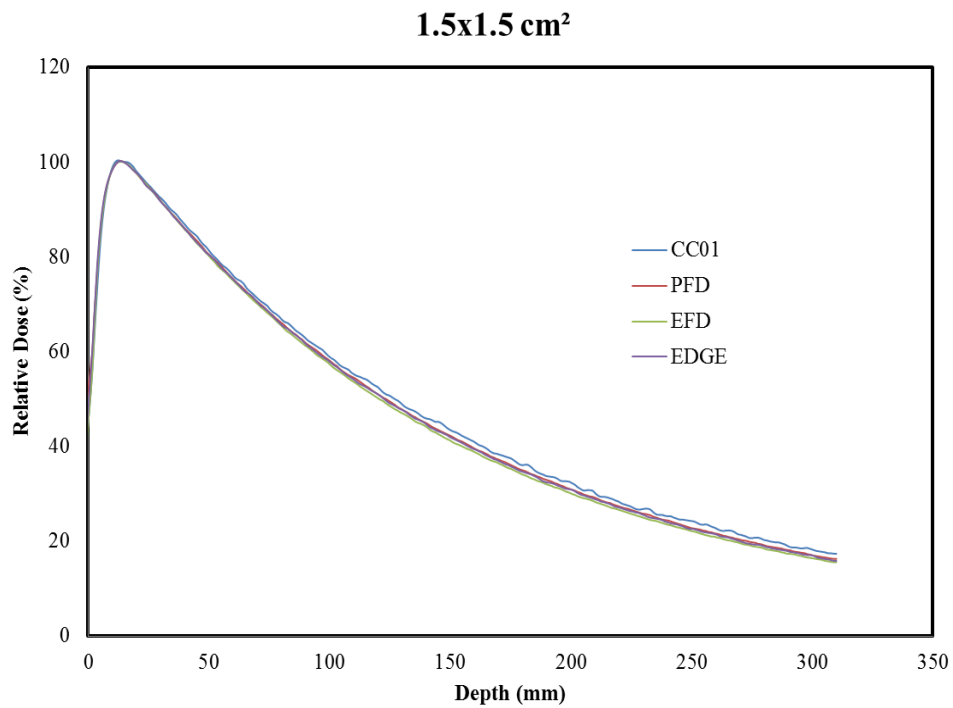
1.5x1.5 cm²

Figure 4.6 Percentage depth doses measured at 100 cm SSD, 10 cm depth, and 1.5x1.5 cm^2 field size using CC01, PFD, EFD, and EDGE.
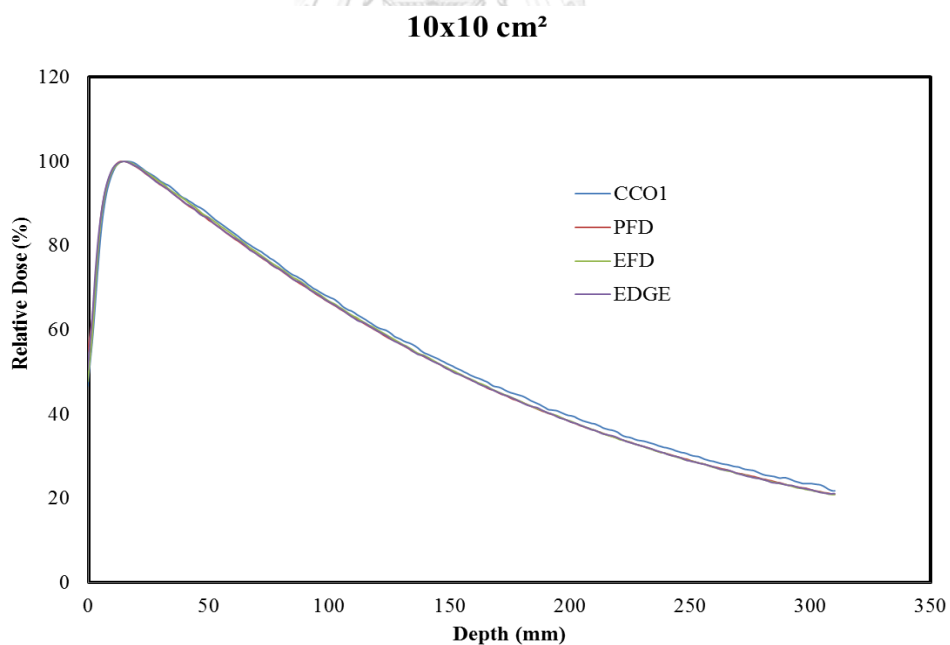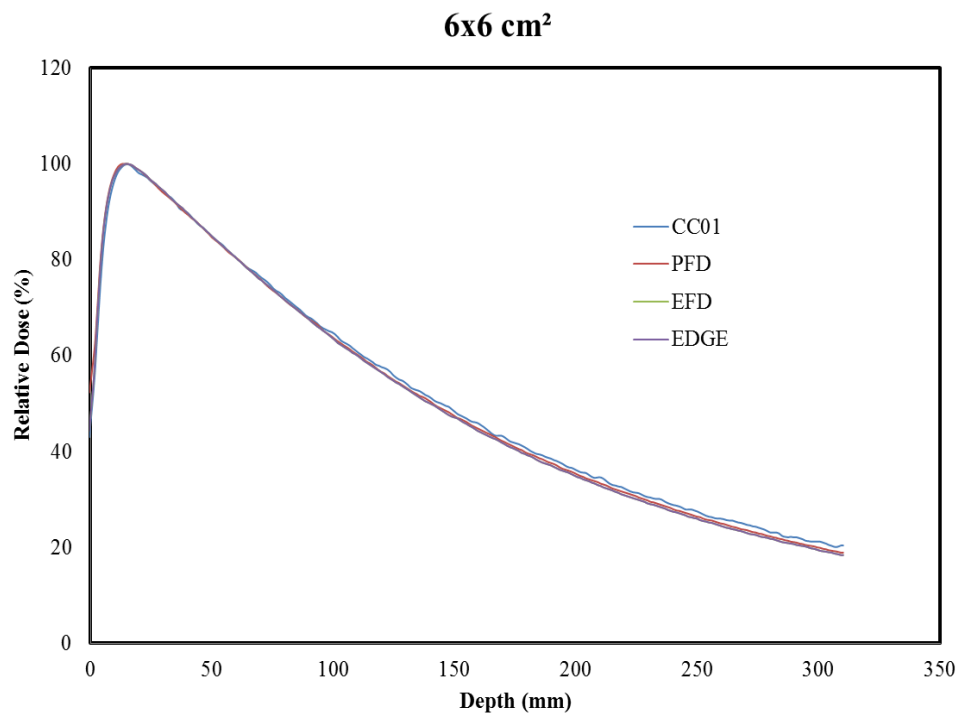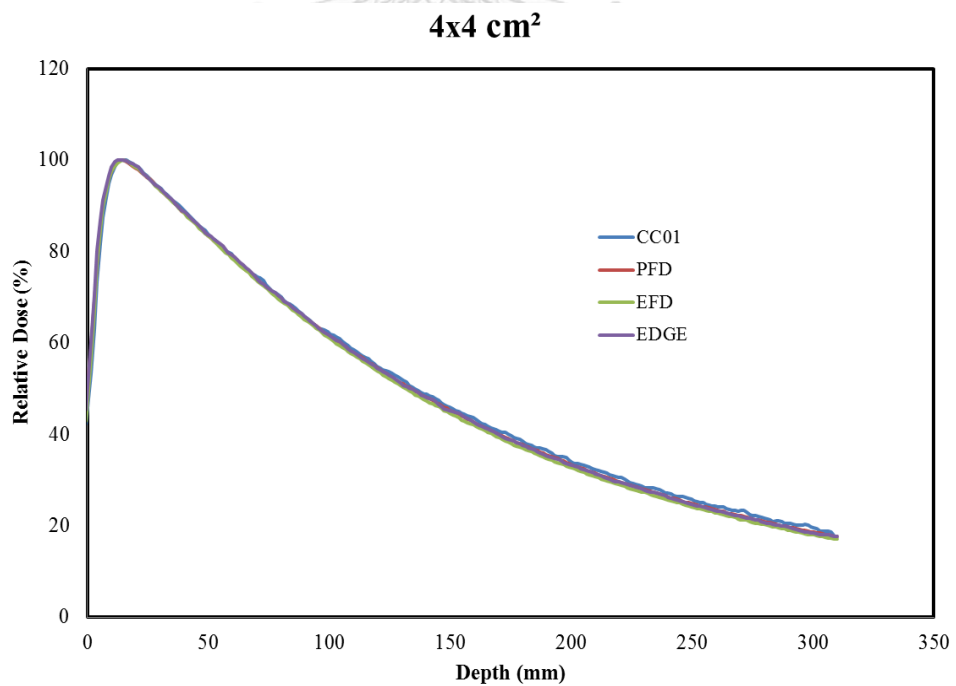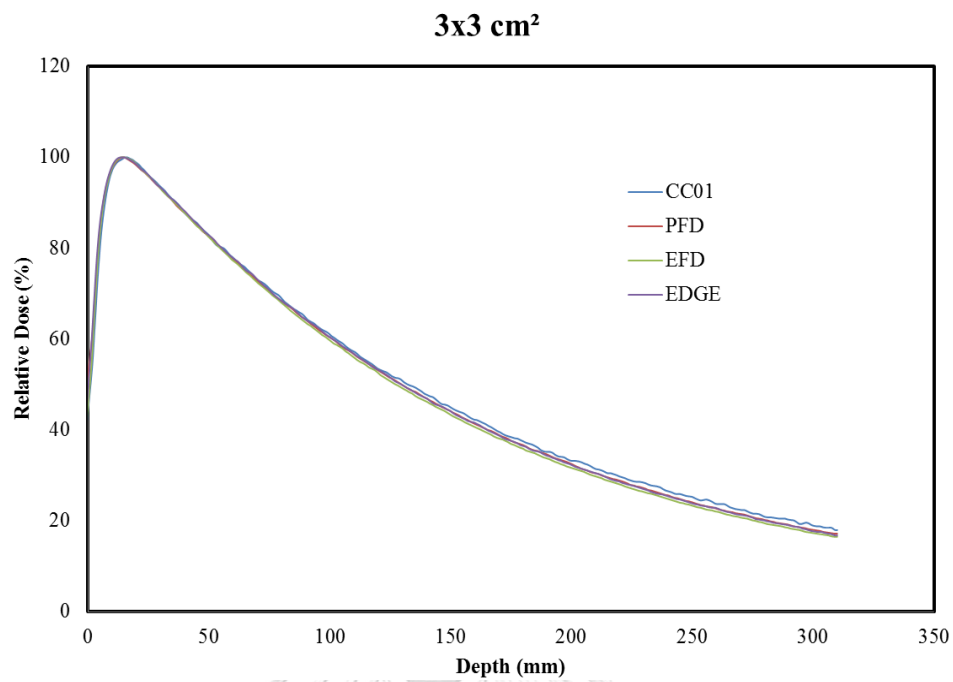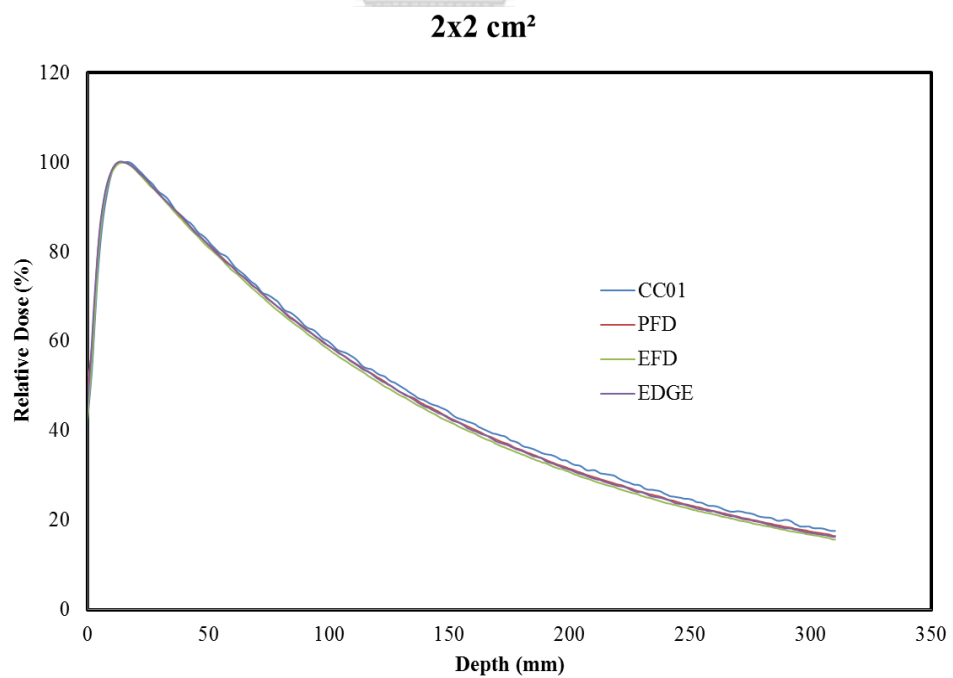
1x1 cm²

Figure 4.7 Percentage depth doses measured at 100 cm SSD, 10 cm depth, and 1x1 cm^2 field size using CC01, PFD, EFD, and EDGE.

Table 4.1 Percentage depth dose of 6 MV photon beams measured at 100 cm SSD and 10 cm depth of measurement using CC01, PFD, EFD, and EDGE.

Side of geometric square field size (cm)	Dose at 10 cm depth (%)				Average±SD	%SD
	CC01	PFD	EFD	EDGE		
10	67.7	66.5	66.9	66.5	66.90±0.6	0.8
6	64.5	63.7	63.5	63.4	63.78±0.5	0.8
4	62.2	61.5	61.3	61.6	61.65±0.4	0.6
3	61.1	60.5	59.8	60.4	60.45±0.5	0.9
2	59.8	58.9	58.2	58.8	58.93±0.7	1.1
1.5	58.8	58.1	57.4	57.8	58.03±0.6	1.0
1	57.7	57.0	56.1	56.6	56.85±0.7	1.2

4.1.2 Beam Profiles

Scanning procedure was continued to the measurement of beam profiles using each detector. Shown in Figure 4.8, 4.9, 4.10, 4.11, 4.12, 4.13, and 4.14, measured profiles at 10x10 cm^2, 6x6 cm^2, 4x4 cm^2, 3x3 cm^2, 2x2 cm^2, 1.5x1.5 cm^2, and 1x1 cm^2 field size. The analysis of penumbra width (cm) 20%-80% isodose line for each beam profile is listed in Table 4.2.

10x10 cm²

Figure 4.8 Beam profiles measured at 100 cm SSD, 10 cm depth, and 10x10 cm^2 field size using CC01, PFD, EFD, and EDGE.

6x6 cm²

Figure 4.9 Beam profiles measured at 100 cm SSD, 10 cm depth, and 6x6 cm^2 field size using CC01, PFD, EFD, and EDGE.
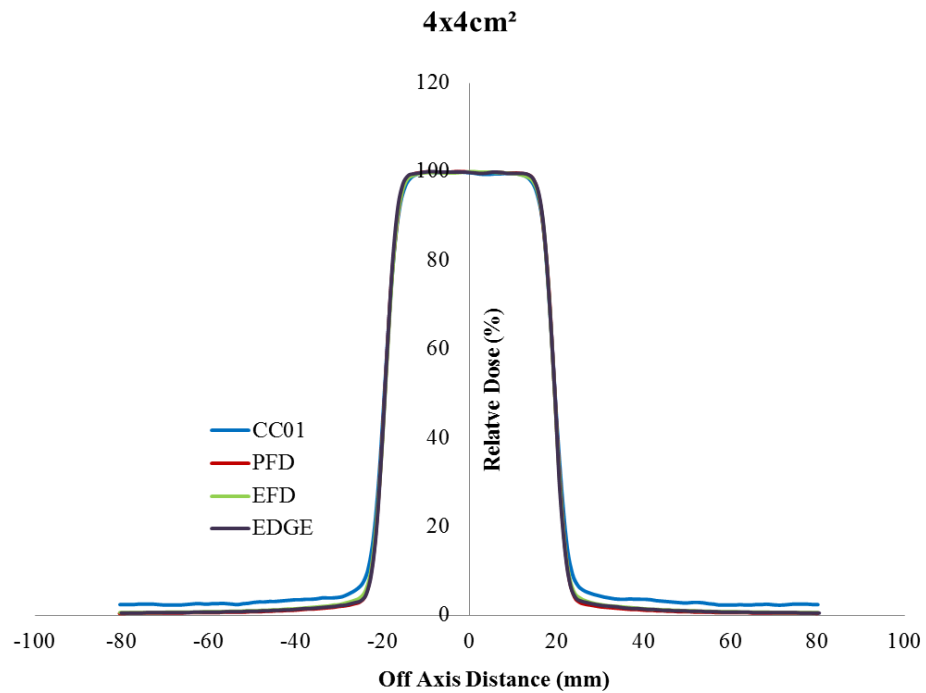
4x4cm²

Figure 4.10 Beam profiles measured at 100 cm SSD, 10 cm depth, and 4x4 cm^2 field size using CC01, PFD, EFD, and EDGE.
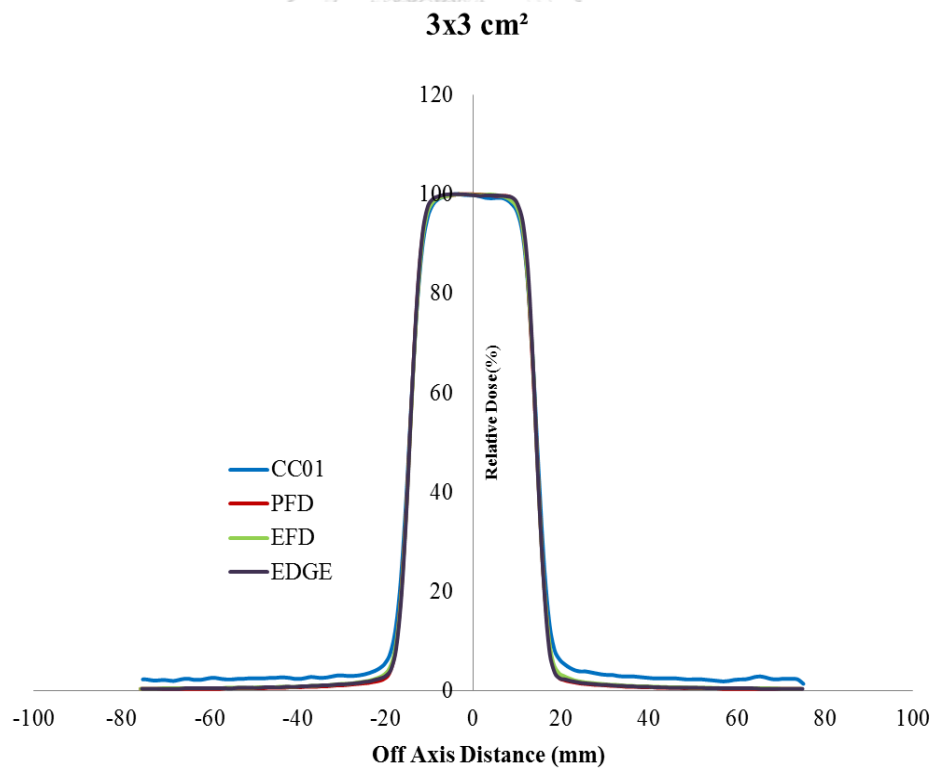
3x3 cm²

Figure 4.11 Beam profiles measured at 100 cm SSD, 10 cm depth, and 3x3 cm^2 field size using CC01, PFD, EFD, and EDGE.
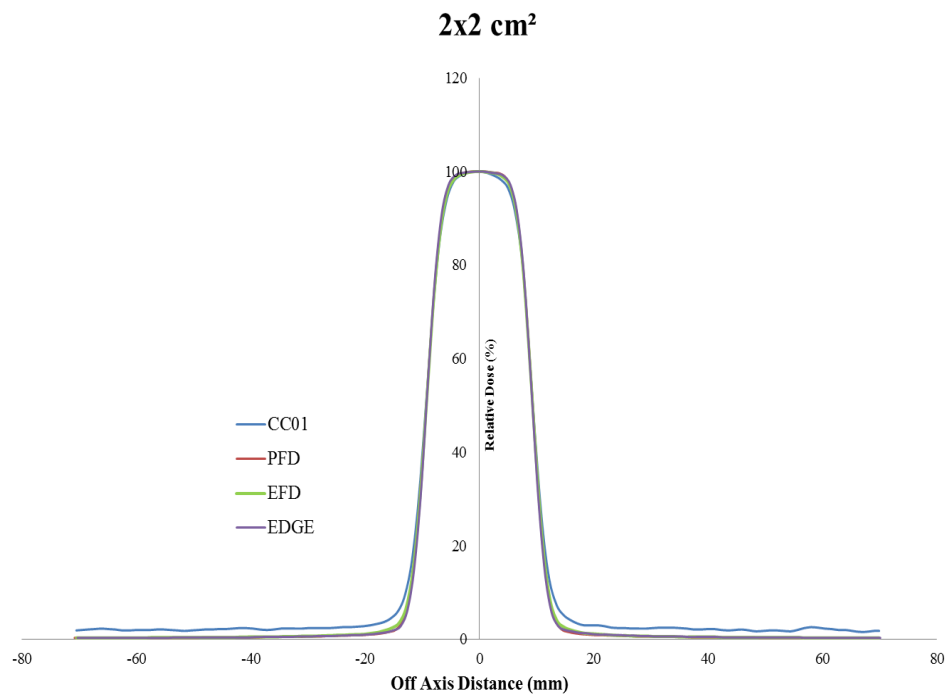
2x2 cm²

Figure 4.12 Beam profiles measured at 100 cm SSD, 10 cm depth, and 2x2 cm^2 field size using CC01, PFD, EFD, and EDGE.
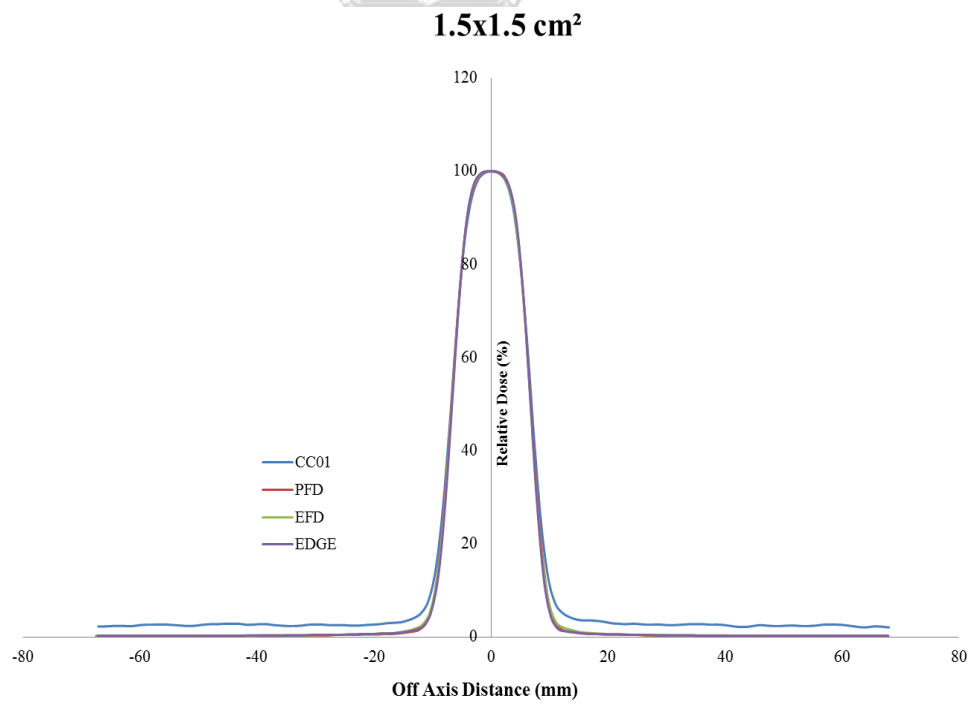
1.5x1.5 cm²

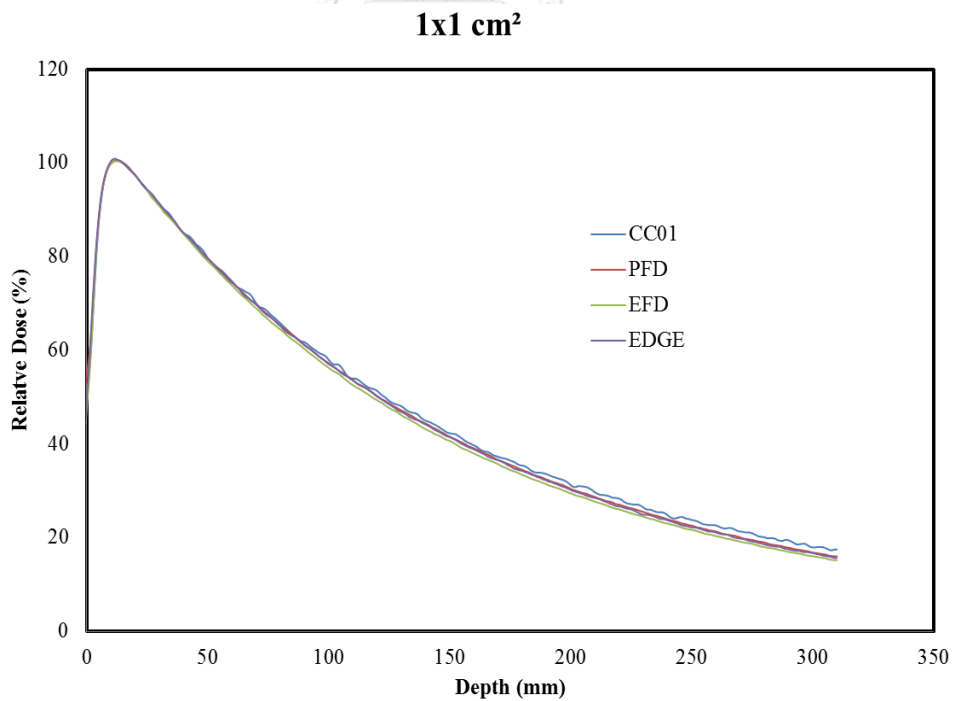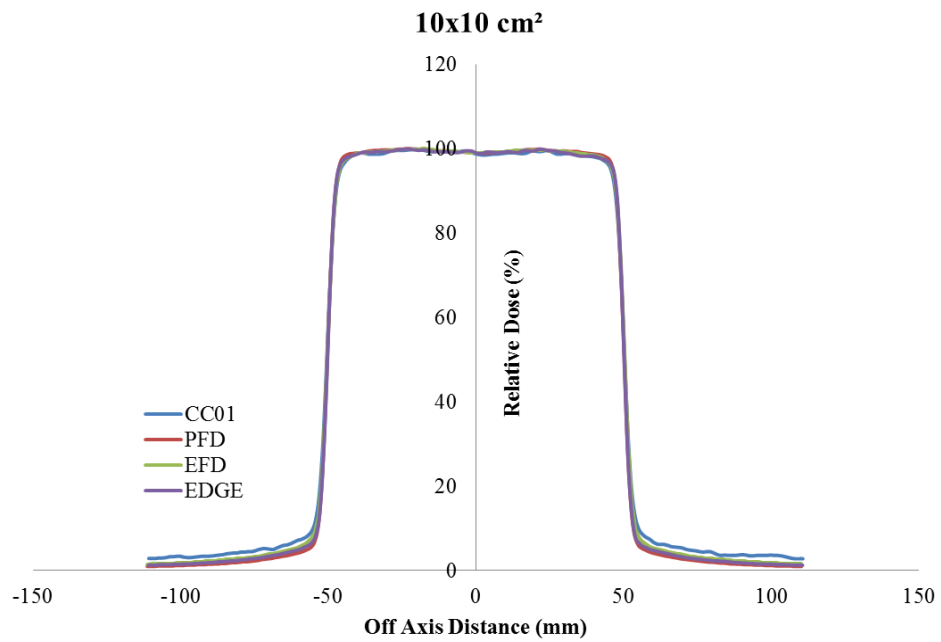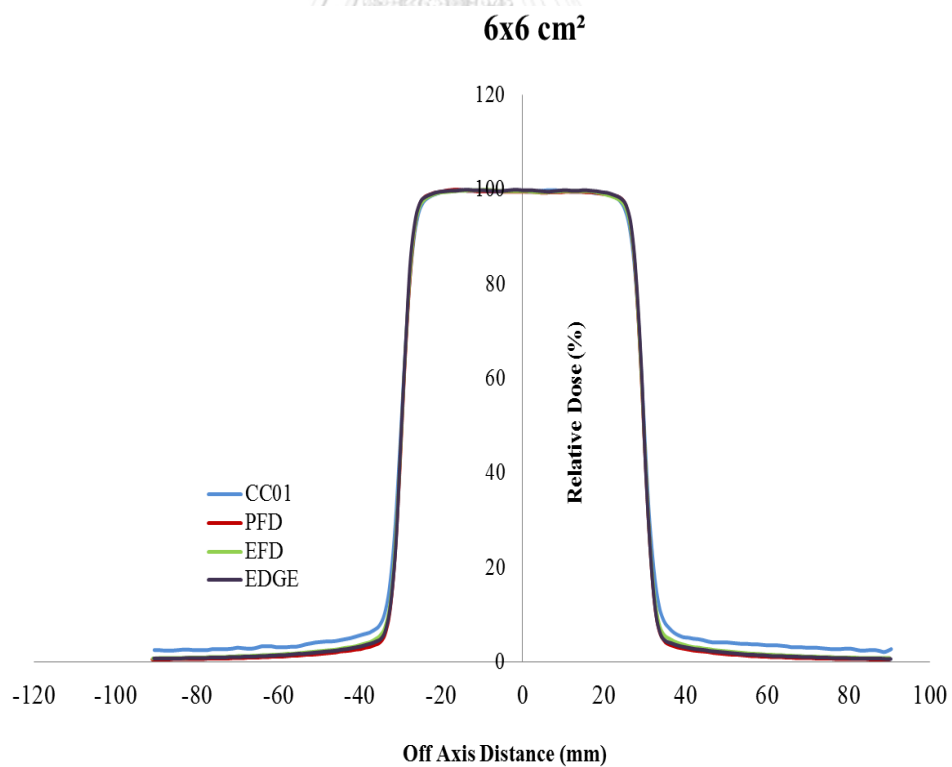Figure 4.13 Beam profiles measured at 100 cm SSD, 10 cm depth, and 1.5x1.5 cm^2 field size using CC01, PFD, EFD, and EDGE.
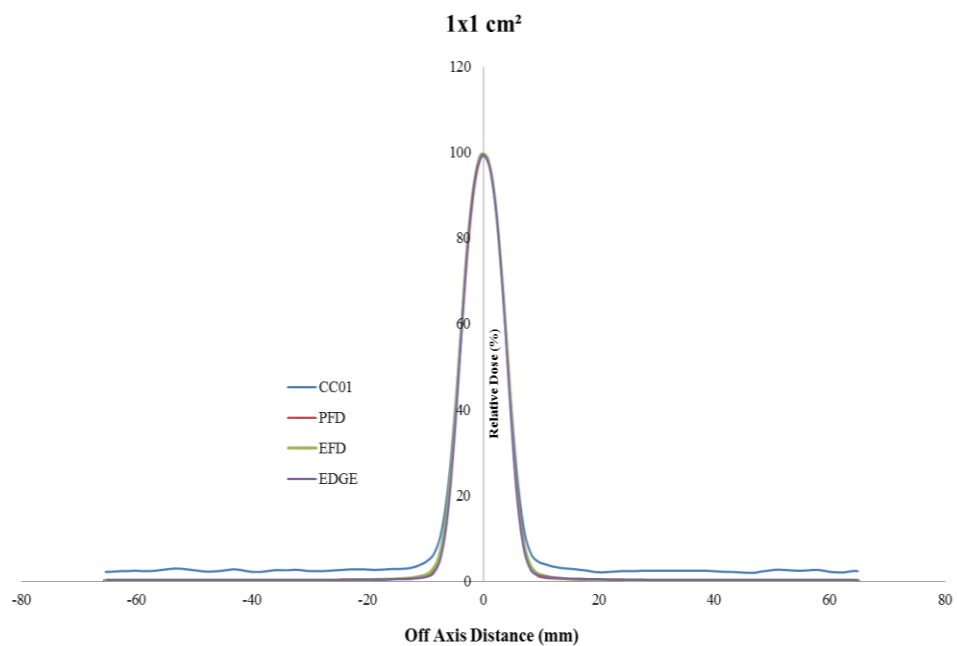
Figure 4.14 Beam profiles measured at 100 cm SSD, 10 cm depth, and 1x1 cm^2 field size using CC01, PFD, EFD, and EDGE.

Table 4.2 Penumbra width (cm) 20%-80% of isodose line measured at 100 cm SSD and depth of maximum dose (d_{max}) using CC01, PFD, EFD, and EDGE.

Side of geometric square field size (cm)	Penumbra width (cm) 20%-80% of isodose line				Average±SD
	CC01	PFD	EFD	EDGE	
10	0.45	0.39	0.40	0.36	0.40±0.04
6	0.44	0.39	0.39	0.35	0.39±0.04
4	0.42	0.38	0.38	0.34	0.38±0.03
3	0.41	0.38	0.37	0.32	0.37±0.04
2	0.40	0.37	0.36	0.32	0.36±0.03
1.5	0.40	0.36	0.34	0.30	0.35±0.04
1	0.36	0.34	0.34	0.23	0.32±0.06

Overall, the differences in percent depth dose at 10 cm depth and penumbra width were found relatively small. For percent depth dose at 10 cm depth, it can be seen that the percent SD in all geometric field sizes were within 1%. For penumbra

width, measurement using CC01 yielded broader penumbra within 0.1 cm compared to the measurement using diode detectors. In addition to that, CC01 was found to yield higher dose in out-of-field region. The outcomes between PFD and EFD were closely matched. Sharper penumbra from EDGE detector was noted.

4.2 Equivalent square field size

Shown in Table 4.3, the dosimetric field width obtained from cross-plane and in-plane direction at reference depth of 10 cm. The equivalent square field size was calculated using equation 3.1.

Table 4.3 The geometric field size along with the corresponding dosimetric field width in the cross-plane and in-plane direction measured at 10 cm depth of FWHM.

Side of geometric square field at 100 cm SSD (cm)	Dosimetric field width at 10 cm depth (cm)		Side of equivalent square field at 10 cm depth (cm)
	Cross-plane	In-plane	
6	6.45	6.63	6.54
4	4.23	4.43	4.33
3	3.12	3.32	3.22
2	2.01	2.20	2.10
1.5	1.46	1.65	1.55
1	0.9	1.11	1.00

4.3 Field output factors

Table 4.4 and Table 4.5 exhibit the uncorrected FOF and corrected FOF determined using CC01, PFD, and EFD, respectively. The average and standard deviation were computed for every field size and reported in the terms of the geometric field size as well as the equivalent square field size of dosimetric field. The comparison between average uncorrected FOF and corrected FOF is plotted in Figure 4.15. Overall, the average difference from all field sizes was less than 1%.

Table 4.4 Uncorrected FOF of 6 MV flattened photon beams measured using CC01, PFD, and EFD.

Side of geometric square field at 100 cm SSD (cm)	FWHM at reference depth (cm)	Uncorrected FOF			Average±SD
		CC01	PFD	EFD	
6	6.54	0.916	0.928	0.908	0.917±0.01
4	4.33	0.859	0.875	0.845	0.860±0.02
3	3.22	0.824	0.844	0.811	0.826±0.02
2	2.10	0.783	0.811	0.771	0.788±0.02
1.5	1.55	0.747	0.786	0.739	0.757±0.03
1	1.00	0.674	0.736	0.668	0.693±0.04

Table 4.5 Corrected FOF of 6 MV flattened photon beams measured using CC01, PFD, and EFD.

Side of geometric square field at 100 cm SSD (cm)	FWHM at reference depth (cm)	Corrected FOF			Average±SD
		CC01	PFD	EFD	
6	6.54	0.919	0.928	0.915	0.921±0.01
4	4.33	0.865	0.874	0.856	0.865±0.01
3	3.22	0.830	0.840	0.824	0.831±0.01
2	2.10	0.790	0.801	0.783	0.791±0.01
1.5	1.55	0.755	0.767	0.748	0.757±0.01
1	1.00	0.686	0.707	0.671	0.688±0.02
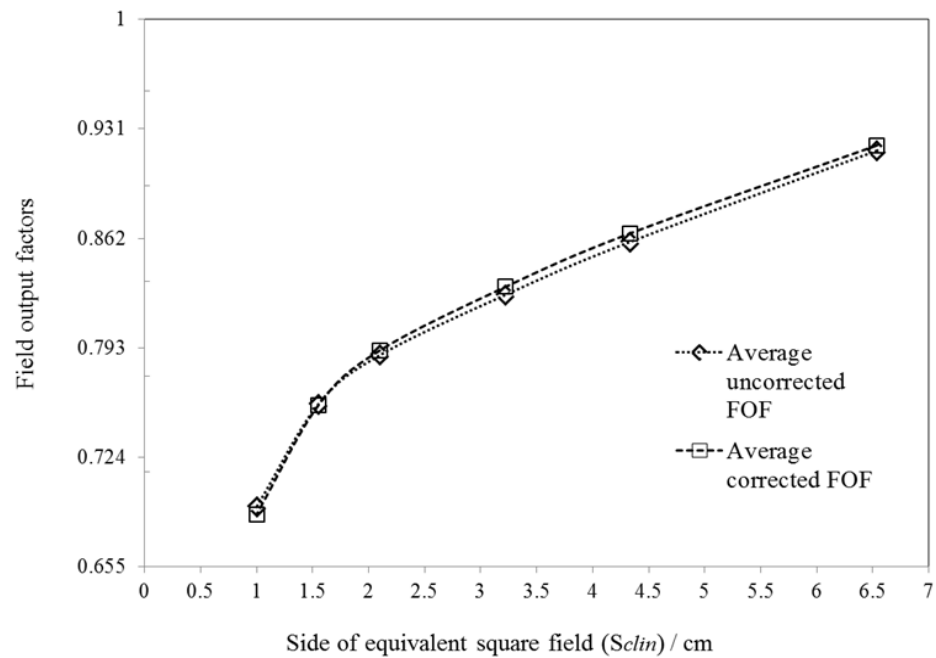
Figure 4.15 Field output factors between average uncorrected FOF and average corrected FOF.

This research highlighted the difference between the use of corrected FOF from single detector and the average uncorrected FOF from three detectors for commissioning small field 6 MV photon beams. In order to do so, the FOF from both conditions were plotted as illustrated in Figure 4.16.
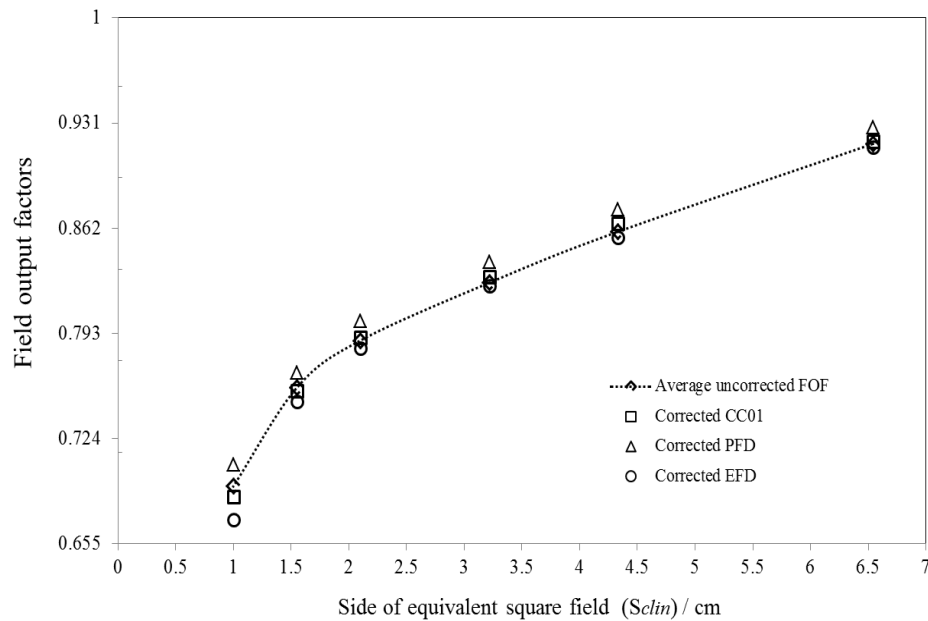
Figure 4.16 Field output factors between single corrected detector and average uncorrected three detectors.

As can be observed from Table 4.4, the PFD demonstrated higher FOF compared to other detectors. On the other hand, the EFD exhibited the lowest FOF while output factors from CC01 were between both diode detectors. The maximum difference was 10% and detected at 1x1 cm^2 field size. CC01, PFD, and EFD exhibited deviation within 3%, 6%, and 4% in the smallest field size compared to the average uncorrected FOF, respectively. The second measurement was completed with the use of field output correction factors based on IAEA/AAPM TRS 483. Despite of implementing the correction factors, the trend remained similar. The outcomes from corrected PFD were consistently higher in comparison to the corrected CC01 and corrected EFD as listed in Table 4.5. However, the difference among detectors at 1x1 cm^2 field size furtherly reduced to 5% compared to the condition without any correction. Compared to the average uncorrected FOF, the percent difference at 1x1 cm² field size was 1%, 2%, and 3% for the corrected CC01, corrected PFD, and corrected EFD, respectively.

4.4 MU Validation

4.4.1 Symmetric field sizes

Observation of calculated MU in Eclipse™ treatment planning system was started from the symmetric field sizes: 1x1 cm^2, 1.5x1.5 cm^2, 2x2 cm^2, 3x3 cm^2, 4x4 cm^2, and 6x6 cm^2 as demonstrated in Figure 4.17. The data of calculated MU for symmetric field sizes is summarized in Appendix I. Overall, the mean differences against commissioning using average FOF as shown in Appendix II were 0.2% (range from -0.7% to 1.5%), -1.6% (range from -2.6% to -0.2%), and 1.2% (range from -0.7% to 3.3%) for commissioning using corrected CC01, corrected PFD, and corrected EFD, respectively. The scatter plot of percentage MU difference as shown in Figure 4.18 clearly shows that the calculated MU was agreeable down to 2x2 cm^2 and started to deviate more at 1.5x1.5 cm^2 field size.

Figure 4.17 Histogram of calculated MU in symmetric field sizes between commissioning using corrected FOF from single detector and average uncorrected FOF from three detectors.

Figure 4.18 Scatter plot of percentage MU differences in symmetric field sizes between commissioning using corrected FOF from single detector and average uncorrected FOF from three detectors.

4.4.2 IMRT-SRS and VMAT-SRS plans

Observation of MU was continued to the IMRT-SRS and VMAT-SRS plans. Shown in Appendix III and Appendix IV, the data of calculated MU for IMRT-SRS as well as the percentage MU differences compared to commissioning using uncorrected FOF. Figure 4.19 and Figure 4.20 depict the histogram of calculated MU and the scatter plot of percent MU differences in IMRT-SRS plans, respectively. The discrepancy exceeding 3% was noted in case number 5 and 8. The mean differences of calculated MU compared to the commissioning using average uncorrected FOF for all cases were -1.3% (range from -3.1% to 0.3%), -3.4% (range from -6.1% to -2%), and -1.5% (range from -4.8% to 2.5%) for commissioning using corrected CC01, corrected PFD, and corrected EFD, respectively. The last observation was made in VMAT-SRS plans. The data is presented in Appendix V and the histogram is displayed in Figure 4.21. Commissioning using corrected CC01 produced an excellent agreement within 0.2% (range from -0.3% to 1.2%) and corrected EFD were also agreeable within -0.2% (range from -0.01% to -0.8%) as can be seen from Figure 4.22 and Appendix VI.

Contrarily, commissioning using corrected PFD exhibited lower MU of -2% (range from -2.5% to -1.3%).

Figure 4.19 Histogram of the calculated MU in IMRT-SRS plans between commissioning using corrected FOF from single detector and average uncorrected FOF from three detectors.

Figure 4.20 Scatter plot of percentage MU differences in IMRT-SRS plans between commissioning using corrected FOF from single detector and average uncorrected FOF from three detectors.
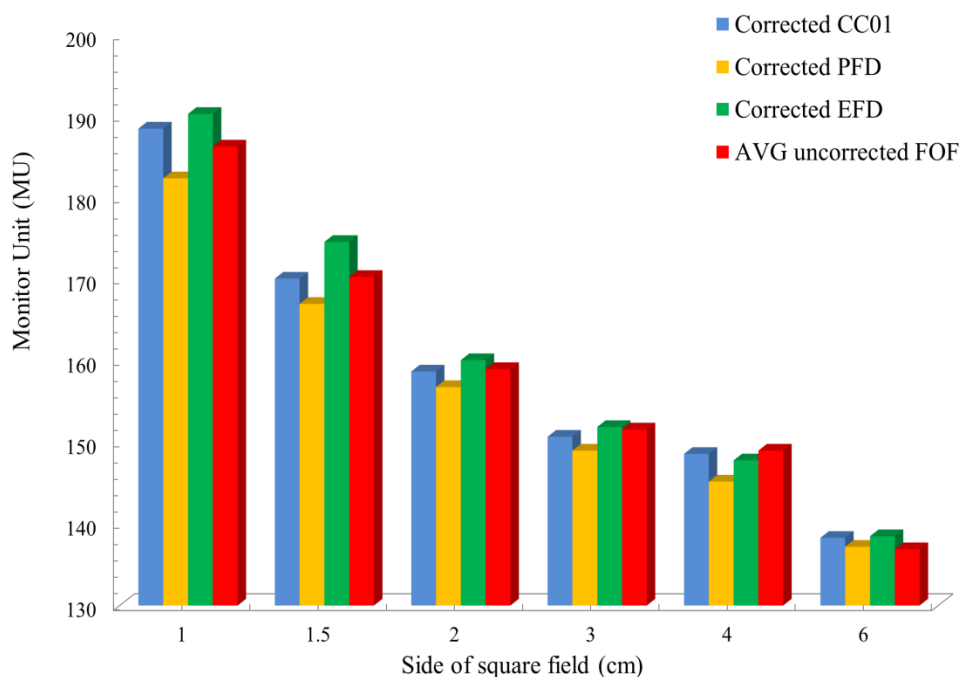
Figure 4.21 Histogram of the calculated MU in VMAT-SRS plans between commissioning using corrected FOF from single detector and average uncorrected FOF from three detectors.
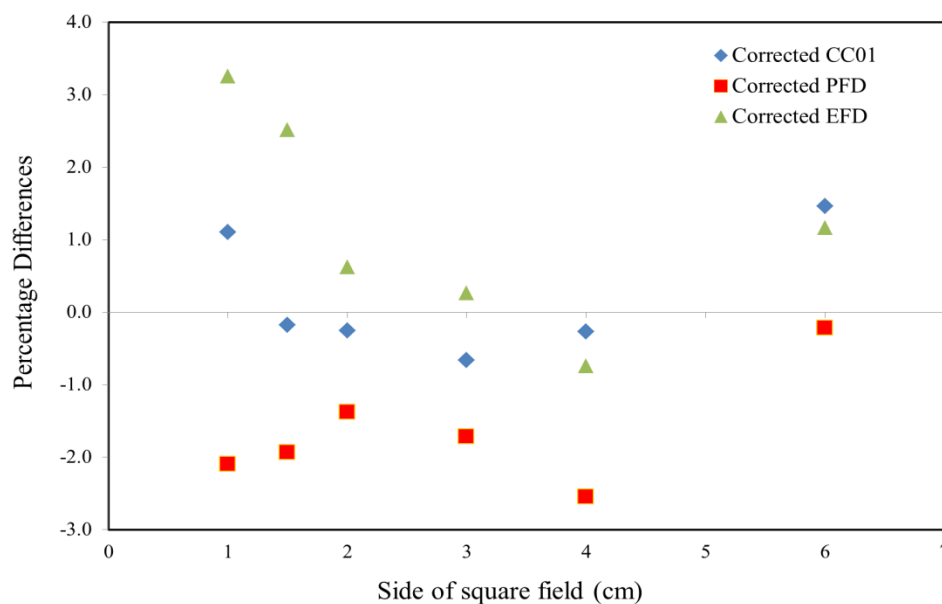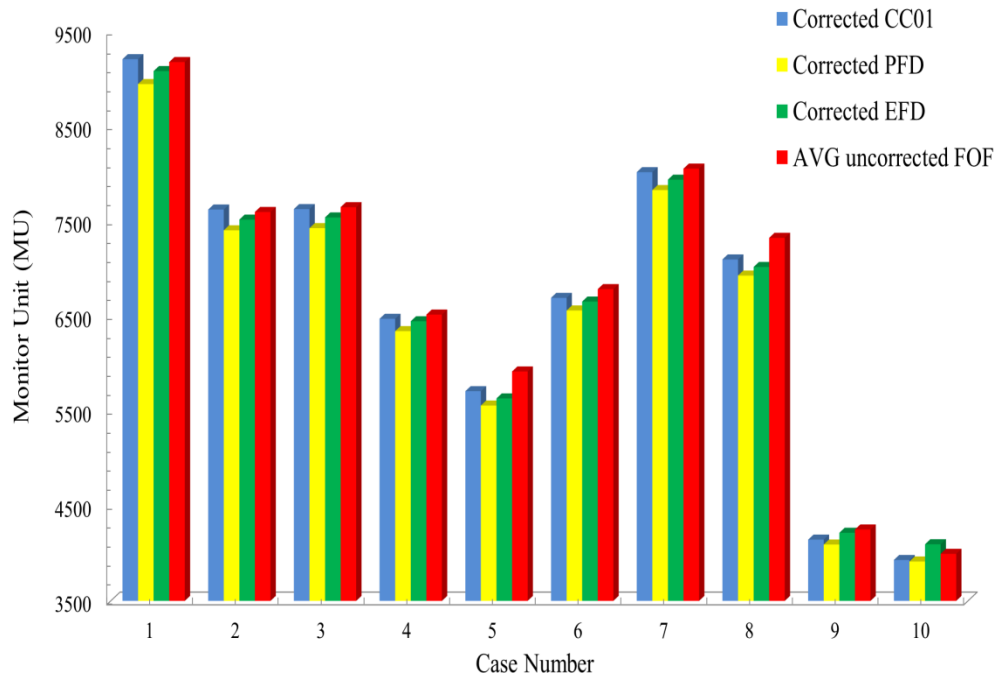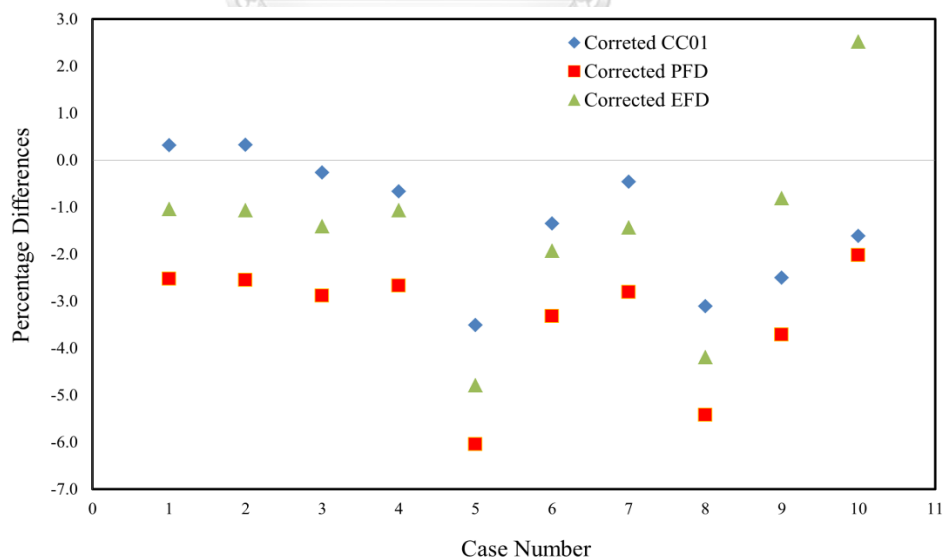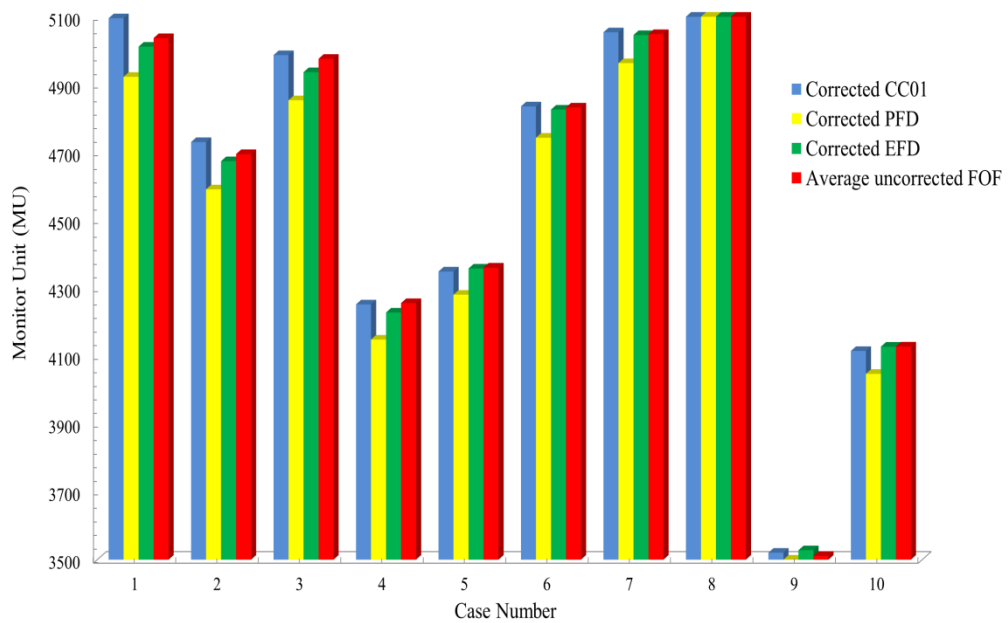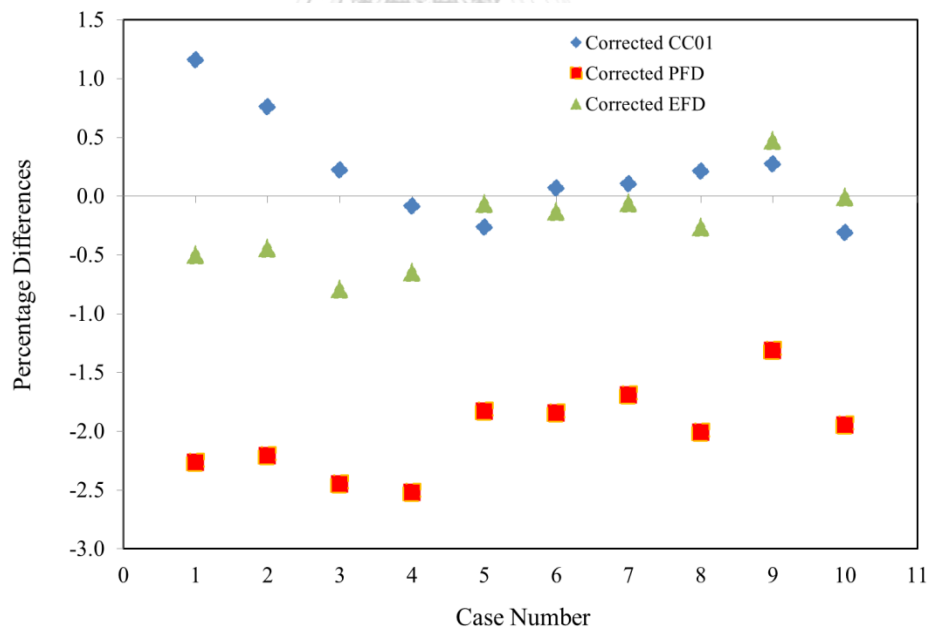

Figure 4.22 Scatter plot of percentage MU differences in VMAT-SRS plans between commissioning using corrected FOF from single detector and average uncorrected FOF from three detectors.

CHAPTER V

DISCUSSION AND CONCLUSION

5.1 Discussion

5.1.1 Percentage depth doses and Beam profiles

Table 4.1 depicts the percent depth dose at 10 cm depth from all detectors. Overall, the outcomes from all detectors were comparable within percent SD of 1%. In particular, PFD and EDGE yielded very close agreement. This result was related to the fact that both detectors were shielded diode detectors. For beam profiles, the lateral distance between 20% and 80% isodose line measured using ionization chamber produced slightly broader penumbra within 0.1 cm than diode detectors as a consequence of volume averaging effect due to the finite size of ion chamber. [36] Once all measured data were incorporated for beam modelling in Eclipse v.11, the outcome was nearly identical. Afterward, measured depth doses and profiles from EDGE detector were appointed as a complementary data for beam commissioning of average uncorrected FOF from three detectors.

5.1.2 Equivalent square field size and Field output factors

For the condition where field sizes do not satisfy the electronic equilibrium, the dosimetric field size will be greater than the actual geometric field size. It is advisable to observe the dosimetric field from FWHM. [3] [37] The dosimetric field as defined from in-plane direction was constantly larger than the cross-plane as previously observed in Table 4.3. The in-plane and cross-plane fields were segmented using the upper jaws and lower jaws, respectively. Inside the Varian treatment head, the upper jaws are closer to the source when compared to the lower jaws and hence resulting into a larger dosimetric field width in the in-plane direction with respect to the greater source occlusion across the upper jaws. [37] EDGE detector was selected to measure the beam profile due to the small active volume and excellent spatial resolution for small field beam scanning. [36] The linear interpolation was used to

assign the appropriate field output correction factors $(k_{Q_{clin}Q_{msr}}^{f_{clin}f_{msr}})$ for each field size based on the corresponding equivalent square field size (S_{clin}).

Prior to the establishment of IAEA/AAPM TRS 483, determination of small field output factors using several detectors has been recommended by several investigators. [3] [9] [33] In this work, three different detectors were employed to determine the FOF: CC01, PFD, and EFD. These detectors are recommended by IAEA/AAPM TRS 483. CC01 represents the recommended ionization chamber while the PFD and EFD represent the recommended diode detectors. After implementing the correction factors according to IAEA/AAPM TRS 483, the deviation among detectors dropped significantly. The corrected PFD, however, still demonstrated higher FOF. This finding was associated to the unwanted scatter from encapsulating component of PFD which possess high density material. [6] [9] [10] [11] Meanwhile, field output factors from EFD unshielded diode presented a good agreement to small field output from CC01. Our result was in line with study from Mc Kerracher et al where they reported an agreeable output factors between measurement using microionization chambers and unshielded diodes. [33] However, our study revealed that it was comparable only until 1.5x1.5 cm^2 field size. Unlike PFD, the EFD contains no high atomic number of shielding material. Instead, the shielding material is replaced with a polymer plastic. [38] It aims to eliminate an excessive electron backscatter from the shielding material into the detection volume.

A good agreement was exhibited between average uncorrected FOF and average corrected FOF in all equivalent square field sizes. This result indicates that field output correction factors $(k_{Q_{clin}Q_{msr}}^{f_{clin}f_{msr}})$ play less important role once multiple recommended detectors such as microionization chambers and diode detectors are available for small field output measurement.

5.1.3 Validation of Monitor Unit (MU)

The accuracy of FOF becomes a critical point to accurately compute the MU in treatment planning system. The relationship is inversely proportional as mentioned in equation 2.2, equation 2.3, and equation 2.4.

For MU validation in symmetric fields, commissioning using corrected PFD steadily produced lower MU as a consequence of higher FOF compared to the average uncorrected FOF from three different detectors. On the other hand, commissioning using CC01 after correction and EFD after correction matched well to the commissioning using average uncorrected FOF. Nevertheless, in field sizes ≤1.5x1.5 cm^2, a large difference within 3% was detected from commissioning using EFD after correction. This result was related to the fact that FOF from corrected EFD yielded lower outcome than the average uncorrected FOF in field sizes ≤1.5x1.5 cm^2.

For MU validation in IMRT-SRS plans, the fluctuation occured and reached large deviation in several cases. The trend, however, was relatively similar where the commissioning using corrected CCO1 yielded the closest agreement within 3%, followed by commissioning using corrected EFD and corrected PFD within 5% and 6%, respectively. The characteristics of IMRT technique to generate higher MU, the complexity of PTV, as well as MLC movement to create multiple small fields are indicated as the main factors influencing our results. For case number 10, the percentage difference from commissioning using corrected EFD started to increase to the positive value and eventually deviated within +2.5%. The PTV of case number 10 was less than 0.5 cm^3 and multiple segmentation fields ≤1.5x1.5 cm^2 were predominantly employed as visualized in Figure 5.1. Therefore, the calculated MU turned to be higher when the FOF was lower than average uncorrected FOF.

For MU validation in VMAT-SRS, two-arcs of gantry rotation were utilized. Unlike IMRT technique which creates non homogeneous dose distributions through several segmented field sizes, the gantry rotation in VMAT technique negates the use of those segmented fields. The smallest case in our study was treated with field size equal to 2x2 cm^2 as illustrated in Figure 5.2. Since the FOF from CC01 after correction and EFD after correction matched well to the average uncorrected FOF at that field, the calculated MU also became comparable within 1%. For commissioning using corrected PFD, a poor agreement was discovered within 2.5% as a consequence of high FOF.
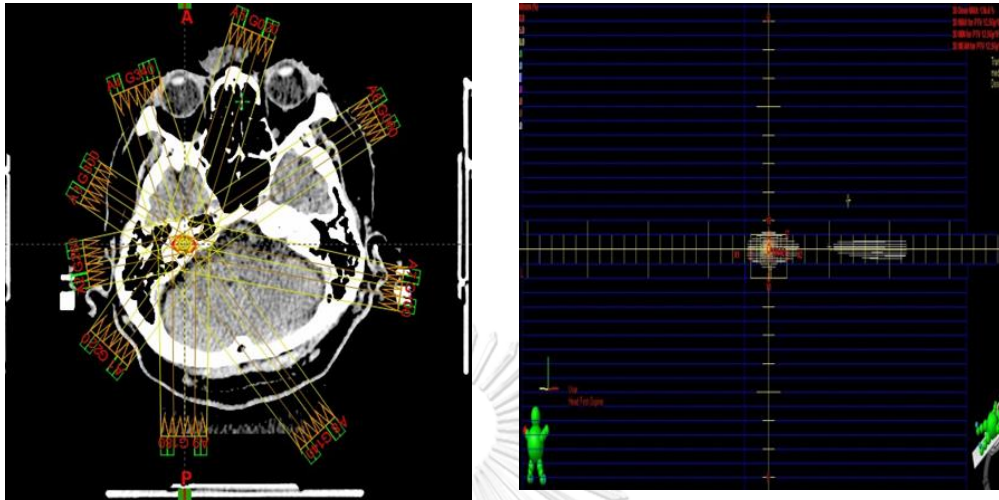
Figure 5. 1 Segmented field size in IMRT-SRS plan equal to approximately 1.5x1.5 cm^2 to treat case number 10 with PTV less than 0.5 cm^3.
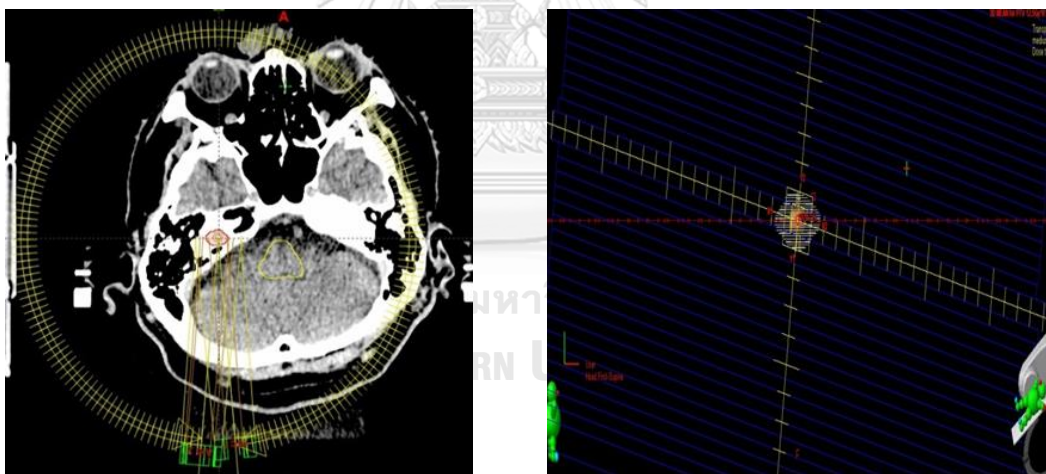
Figure 5. 2 Segmented field size in VMAT-SRS plan equal to approximately 2x2 cm^2 to treat case number 10 with PTV less than 0.5 cm^3.

The limitation of this work was attributed to the commissioning process in Eclipse^{TM} where we were unable to incorporate the small field output less than 1x1 cm^2. For smaller fields, Eclipse^{TM} did extrapolation itself which went out from our scope. Validation of MU in other treatment planning system would be initiated for the future work.

5.2 Conclusion

5.2.1 Conclusion

As a conclusion remark in this research, Table 5.1 exhibits the percent mean differences of calculated MU from all commissioning datasets compared to commissioning using average uncorrected FOF from three detectors. Commissioning 6 MV flattened photon beams using CC01 after correction based on IAEA/AAPM TRS 483 agreed well to the commissioning using average uncorrected FOF from three different detectors to calculate MU in Eclipse™ treatment planning system within maximum difference of -3.1%.

Table 5.1 Percent mean differences from all commissioning datasets compared to commissioning using average uncorrected FOF from three detectors to calculate MU.

Types of commissioning	Symmetric field sizes	IMRT-SRS plans	VMAT-SRS plans
Corrected CC01	**0.2%** (range from -0.7% to 1.5%)	**-1.3%** (range from -3.1% to 0.3%)	**0.2%** (range from -0.3% to 1.2%)
Corrected PFD	**-1.6%** (range from -2.6% to -0.2%)	**-3.4%** (range from -6.1% to -2%)	**-2%** (range from -2.5% to -1.3%)
Corrected EFD	**1.2%** (range from -0.7% to 3.3%)	**-1.5%** (range from -4.8% to 2.5%)	**-0.2%** (range from -0.01% to -0.8%)

5.2.2 Suggestion

No single detector is finally enough to accommodate small field dosimetry. The use of several detectors for beam data acquisition in small field is recommended to ensure the accuracy of measured data before commissioning process in the treatment planning system. This research recommends the use of diode detector with small active volume for beam scanning. Meanwhile, the detector choice for small field output measurement is small ionization chamber along with the implementation of correction factors based on IAEA/AAPM TRS 483.

REFERENCES

1. Lutz, W., K.R. Winston, and N. Maleki, *A system for stereotactic radiosurgery with a linear accelerator.* International Journal of Radiation Oncology• Biology• Physics, 1988. **14**(2): p. 373-381.

2. Levivier, M., T. Gevaert, and L. Negretti, *Gamma Knife, CyberKnife, TomoTherapy: gadgets or useful tools?* Current opinion in neurology, 2011. **24**(6): p. 616-625.

3. Das, I.J., G.X. Ding, and A. Ahnesjö, *Small fields: nonequilibrium radiation dosimetry.* Medical physics, 2008. **35**(1): p. 206-215.

4. IAEA, T., *483. Dosimetry of small static fields used in external beam radiotherapy: An IAEA-AAPM international code of practice for reference and relative dose determination,* Technical Report Series.

5. Das, I.J., et al., *Choice of radiation detector in dosimetry of stereotactic radiosurgery-radiotherapy.* Journal of Radiosurgery, 2000. **3**(4): p. 177-186.

6. Cranmer-Sargison, G., et al., *Experimental small field 6 MV output ratio analysis for various diode detector and accelerator combinations.* Radiotherapy and Oncology, 2011. **100**(3): p. 429-435.

7. Wuerfel, J., *Dose measurements in small fields.* Med Phys, 2013. **1**(1): p. 81-90.

8. Laub, W.U. and T. Wong, *The volume effect of detectors in the dosimetry of small fields used in IMRT.* Medical physics, 2003. **30**(3): p. 341-347.

9. Kairn, T., et al., *Clinical use of diodes and micro-chambers to obtain accurate small field output factor measurements.* Australasian physical & engineering sciences in medicine, 2015. **38**(2): p. 357-367.

10. Azangwe, G., et al., *Detector to detector corrections: a comprehensive experimental study of detector specific correction factors for beam output measurements for small radiotherapy beams.* Medical physics, 2014. **41**(7).

11.   Ralston, A., et al., *Small field diode correction factors derived using an air core fibre optic scintillation dosimeter and EBT2 film.* Physics in Medicine & Biology, 2012. **57**(9): p. 2587.

12.   Alfonso, R., et al., *A new formalism for reference dosimetry of small and nonstandard fields.* Medical physics, 2008. **35**(11): p. 5179-5186.

13.   Gibbons, J.P., et al., *Monitor unit calculations for external photon and electron beams: Report of the AAPM Therapy Physics Committee Task Group No. 71.* Medical physics, 2014. **41**(3).

14.   J.Seuntjens, E.F.L., S.Cora, G.X.Ding, *Prescribing, Recording, and Reporting of Stereotactic Treatments with Small Photon Beams ICRU Report N0.91.* Journal of the International Commission on Radiation Units and Measurements, 2017. **14**(2): p. 1-160.

15.   Underwood, R.J., *Small field dose measurements with Gafchromic film*, 2013, Georgia Institute of Technology.

16.   Khan, F. and J. Gibbons, *Khan's the physics of radiation therapy. 2014.* Google Scholar.

17.   Li, X.A., et al., *Lateral electron equilibrium and electron contamination in measurements of head-scatter factors using miniphantoms and brass caps.* Medical physics, 1995. **22**(7): p. 1167-1170.

18.   Low, D.A., et al., *Ionization chamber volume averaging effects in dynamic intensity modulated radiation therapy beams.* Medical physics, 2003. **30**(7): p. 1706-1711.

19.   Van Dyk, J., et al., *Commissioning and quality assurance of treatment planning computers.* International Journal of Radiation Oncology* Biology* Physics, 1993. **26**(2): p. 261-273.

20.   Das, I.J., et al., *Accelerator beam data commissioning equipment and procedures: report of the TG-106 of the therapy physics committee of the AAPM.* Igaku butsuri: Nihon Igaku Butsuri Gakkai kikanshi= Japanese journal of medical physics: an official journal of Japan Society of Medical Physics, 2013. **33**(1): p. 16.

21. Fraass, B., et al., *American Association of Physicists in Medicine Radiation Therapy Committee Task Group 53: quality assurance for clinical radiotherapy treatment planning.* Medical physics, 1998. **25**(10): p. 1773-1829.

22. Ganz, J.C., *Gamma knife radiosurgery and its possible relationship to malignancy: a review.* Journal of neurosurgery, 2002. **97**: p. 644-652.

23. Deodato, F., et al., *Stereotactic radiosurgery (SRS) with volumetric modulated arc therapy (VMAT): interim results of a multi-arm phase I trial (DESTROY-2).* Clinical Oncology, 2014. **26**(12): p. 748-756.

24. Cuaron, J.J., et al., *Stereotactic body radiation therapy for primary lung cancers> 3 centimeters.* Journal of Thoracic Oncology, 2013. **8**(11): p. 1396-1401.

25. Mayles, P., A.E. Nahum, and J.-C. Rosenwald, *Handbook of radiotherapy physics: theory and practice.* 2007: CRC Press.

26. Ezzell, G.A., et al., *IMRT commissioning: multiple institution planning and dosimetry comparisons, a report from AAPM Task Group 119.* Medical physics, 2009. **36**(11): p. 5359-5373.

27. Han, T., et al., *Dosimetric comparison of Acuros XB deterministic radiation transport method with Monte Carlo and model ‑based convolution methods in heterogeneous media.* Medical physics, 2011. **38**(5): p. 2651-2664.

28. Hoffmann, L., et al., *Clinical validation of the Acuros XB photon dose calculation algorithm, a grid-based Boltzmann equation solver.* Acta oncologica, 2012. **51**(3): p. 376-385.

29. Derreumaux, S., et al. *Concerns in France over the Dose Delivered to the Patients in Stereotactic Radiation Therapy.* in *Standards, Applications and Quality Assurance in Medical Radiation Dosimetry (IDOS). Proceedings of an International Symposium. V. 1.* 2011.

30. Benmakhlouf, H., J. Sempau, and P. Andreo, *Output correction factors for nine small field detectors in 6 MV radiation therapy photon beams: a PENELOPE Monte Carlo study.* Medical physics, 2014. **41**(4).

31. Podgorsak, E., *Radiation oncology physics: a handbook for teachers and students.* British journal of cancer, 2008. **98**(5): p. 71-99.

32. Griessbach, I., et al., *Dosimetric characteristics of a new unshielded silicon diode and its application in clinical photon and electron beams.* Medical physics, 2005. **32**(12): p. 3750-3754.

33. McKerracher, C. and D. Thwaites, *Assessment of new small-field detectors against standard-field detectors for practical stereotactic beam data acquisition.* Physics in Medicine & Biology, 1999. **44**(9): p. 2143.

34. García-Garduño, O., et al., *Effect of dosimeter type for commissioning small photon beams on calculated dose distribution in stereotactic radiosurgery.* Medical physics, 2014. **41**(9).

35. Andreo, P., et al., *IAEA TRS-398. Absorbed dose determination in external beam radiotherapy: an international code of practice for dosimetry based on standards of absorbed dose to water.* International Atomic Energy Agency, 2000.

36. Gersh, J.A., R. Best, and R.J. Watts, *The clinical impact of detector choice for beam scanning.* Journal of applied clinical medical physics, 2014. **15**(4): p. 174-193.

37. Cranmer-Sargison, G., et al., *A methodological approach to reporting corrected small field relative outputs.* Radiotherapy and Oncology, 2013. **109**(3): p. 350-355.

38. Pantelis, E., et al., *On the output factor measurements of the CyberKnife iris collimator small fields: Experimental determination of the kQclin, Qmsrfclin, fmsr correction factors for microchamber and diode detectors.* Medical physics, 2012. **39**(8): p. 4875-4885.

APPENDIX

Appendix I. Calculated MU in symmetric field sizes.

Side of symmetric field size (cm)	Commissioning using corrected CC01	Commissioning using corrected PFD	Commissioning using corrected EFD	Commissioning using average uncorrected FOF	%SD
6	138.3	137.2	138.5	136.9	0.6
4	148.6	145.2	147.8	149.0	1.2
3	150.7	149.0	151.9	151.6	0.9
2	158.7	156.8	160.1	159.0	0.9
1.5	170.1	167.0	174.6	170.3	1.8
1	188.5	182.4	190.3	186.3	1.8

Appendix II. Percentage differences of calculated MU in symmetric field sizes compared to commissioning using average uncorrected FOF.

Side of symmetric field size (cm)	Commissioning using corrected CC01	Commissioning using corrected PFD	Commissioning using corrected EFD
6	1.0	0.2	1.2
4	-0.3	-2.6	-0.8
3	-0.6	-1.7	0.2
2	-0.2	-1.4	0.7
1.5	-0.1	-1.9	2.5
1	1.2	-2.1	2.1

Appendix III. Calculated MU in IMRT-SRS plans.

Case Number	Volume (cc)	Commissioning using corrected CC01	Commissioning using corrected PFD	Commissioning using corrected EFD	Commissioning using average uncorrected FOF	%SD
1	14.06	9203.7	8942.2	9078.9	9174.4	1.3
2	13.03	7620.4	7401.8	7514.8	7595.8	1.3
3	11.16	7626.0	7424.9	7538.2	7645.9	1.3
4	6.31	6470.8	6340.2	6444.6	6514.2	1.1
5	3.01	5707.7	5557.4	5631.8	5915.4	2.7
6	2.67	6691.2	6557.7	6652.2	6782.9	1.4
7	1.86	8014.2	7825.2	7935.4	8051.2	1.3
8	1.62	7095.5	6926.0	7015.9	7323.3	2.4
9	0.78	4144.9	4093.4	4216.9	4251.4	1.7
10	0.36	3931.1	3914.7	4096.3	3995.6	2.1

Appendix IV. Percentage differences of calculated MU in IMRT-SRS plans compared to commissioning using average uncorrected FOF.

Case Number	Commissioning using corrected CC01	Commissioning using corrected PFD	Commissioning using corrected EFD
1	0.3	-2.5	-1.0
2	0.3	-2.6	-1.1
3	-0.3	-2.9	-1.4
4	-0.7	-2.7	-1.1
5	-3.5	-6.1	-4.8
6	-1.4	-3.3	-1.9
7	-0.5	-2.8	-1.4
8	-3.1	-5.4	-4.2
9	-2.5	-3.7	-0.8
10	-1.6	-2.0	2.5

Appendix V. Calculated MU in VMAT-SRS plans.

Case Number	Volume (cc)	Commissioning using corrected CC01	Commissioning using corrected PFD	Commissioning using corrected EFD	Commissioning using average uncorrected FOF	%SD
1	14.06	5095.5	4922.9	5011.8	5037.0	1.4
2	13.03	4730.7	4591.3	4674.4	4695.2	1.3
3	11.16	4986.9	4853.9	4936.6	4976.0	1.2
4	6.31	4252.3	4148.6	4228.3	4256.0	1.2
5	3.01	4349.2	4280.8	4357.9	4360.7	0.9
6	2.67	4835.8	4743.5	4826.3	4832.6	0.9
7	1.86	5054.1	4963.3	5046.0	5048.9	0.9
8	1.62	7135.4	6977.4	7101.5	7120.4	1.0
9	0.78	3520.6	3464.9	3527.7	3511.1	0.8
10	0.36	4115.0	4047.6	4127.7	4128.0	0.9

Appendix VI. Percentage differences of calculated MU in VMAT-SRS plans compared to commissioning using average uncorrected FOF.

Case Number	Commissioning using corrected CC01	Commissioning using corrected PFD	Commissioning using corrected EFD
1	1.2	-2.3	-0.5
2	0.8	-2.2	-0.4
3	0.2	-2.5	-0.8
4	-0.1	-2.5	-0.6
5	-0.3	-1.8	-0.1
6	0.1	-1.8	-0.1
7	0.1	-1.7	-0.3
8	0.2	-2.0	0.5
9	0.3	-1.3	-0.01
10	-0.3	-1.9	-0.2

VITA

Mr. Sammuel Mamesa was born in Pandeglang, Banten, Indonesia on 12th of July 1991. He obtained his undergraduate degree in Physics in the year of 2013 from Faculty of Science and Mathematics, Diponegoro University, Indonesia. Under H.M The King Bhumibol Adulyadej 72nd Scholarship for International Students, he accomplished M.Sc degree in Medical Imaging from Faculty of Medicine, Chulalongkorn University, Thailand in 2018. He is available at sammuelmedphys@gmail.com.